Sun *et al. Microbiome* (2025) 13:126
https://doi.org/10.1186/s40168-025-02120-y

Microbiome

RESEARCH

Open Access

Interactions with native microbial keystone taxa enhance the biocontrol efficiency of *Streptomyces*

Tianyu Sun[1†], Hongwei Liu[2,3†], Ningqi Wang[1], Mingcong Huang[1], Samiran Banerjee[4], Alexandre Jousset[1], Yangchun Xu[1], Qirong Shen[1], Shimei Wang[1*], Xiaofang Wang[1*] and Zhong Wei[1*]

Abstract

Background *Streptomyces* spp. are known for producing bioactive compounds that suppress phytopathogens. However, previous studies have largely focused on their direct interactions with pathogens and plants, often neglecting their interactions with the broader soil microbiome. In this study, we hypothesized that these interactions are critical for effective pathogen control. We investigated a diverse collection of *Streptomyces* strains to select those with strong protective capabilities against tomato wilt disease caused by *Ralstonia solanacearum*. Leveraging a synthetic community (SynCom) established in our lab, alongside multiple *in planta* and in vitro co-cultivation experiments, as well as transcriptomic and metabolomic analyses, we explored the synergistic inhibitory mechanisms underlying bacterial wilt resistance facilitated by both *Streptomyces* and the soil microbiome.

Results Our findings indicate that direct antagonism by *Streptomyces* is not sufficient for their biocontrol efficacy. Instead, the efficacy was associated with shifts in the rhizosphere microbiome, particularly the promotion of two native keystone taxa, CSC98 (*Stenotrophomonas maltophilia*) and CSC13 (*Paenibacillus cellulositrophicus*). *In vitro* co-cultivation experiments revealed that CSC98 and CSC13 did not directly inhibit the pathogen. Instead, the metabolite of CSC13 significantly enhanced the inhibition efficiency of *Streptomyces* R02, a highly effective biocontrol strain in natural soil. Transcriptomic and metabolomic analyses revealed that CSC13's metabolites induced the production of Erythromycin E in *Streptomyces* R02, a key compound that directly suppressed *R. solanacearum*, as demonstrated by our antagonism tests.

Conclusions Collectively, our study reveals how beneficial microbes engage with the native soil microbiome to combat pathogens, suggesting the potential of leveraging microbial interactions to enhance biocontrol efficiency. These findings highlight the significance of intricate microbial interactions within the microbiome in regulating plant diseases and provide a theoretical foundation for devising efficacious biocontrol strategies in sustainable agriculture.

Keywords Tomato bacterial wilt, *Streptomyces*, Synthetic community, *Stenotrophomonas*, *Paenibacillus*, Microbial interaction, Multi-omics analysis

†Tianyu Sun and Hongwei Liu contributed equally to this work.

*Correspondence:
Shimei Wang
smwang@njau.edu.cn
Xiaofang Wang
wangxf@niau.edu.cn
Zhong Wei
weizhong@njau.edu.cn
Full list of author information is available at the end of the article

Introduction

The rhizosphere is a vibrant microecosystem teeming with a multitude of microorganisms, including bacteria, archaea, fungi, and other eukaryotes, playing a pivotal role in plant health and soil fertility [1]. These microorganisms engage in intricate interactions that significantly influence plant growth and stress tolerance [2, 3]. Notable among them are microbes such as *Bacillus* spp. and *Streptomyces* spp., which are known for producing beneficial compounds, such as siderophores and phytohormones that have been extensively studied for their potential as biocontrol agents [4, 5]. Recently, the European Union has approved *Streptomyces lydicus* WYEC for biocontrol purposes in agricultural fields due to its ability to inhibit various fungal plant pathogens [6]. Despite their potential as biocontrol agents and eco-friendly alternatives to synthetic fungicides, the practical implementation in field conditions faces several hurdles [7]. One major challenge is the unpredictable efficacy, which can fluctuate significantly due to various factors, including soil composition, crop types, and weather conditions [7, 8]. Additionally, our understanding of the intricate relationships between biocontrol microorganisms and the native soil microbiota, as well as the consequent impact on biocontrol performance, is still limited [9, 10]. This knowledge gap restricts our ability to formulate effective biocontrol inoculants for different agricultural settings.

Metabolite-driven microbial interactions make the rhizosphere a dynamic ecological hotspot. Rhizosphere microbes produce a diverse array of secondary metabolites, such as siderophores (e.g., coelichelin and desferrioxamine) [11], detoxification enzymes (e.g., catalase and mercuric ion reductase) [12, 13], and specialized bioactive compounds of chresdihydrochalcone, chresphenylacetone, streptimidone, and lipopeptide [14, 15]. Additionally, they release crucial primary metabolites like amino acids (e.g., methionine, lysine, isoleucine, and arginine) [16]. *Streptomyces* spp. are particularly recognized as effective biocontrol agents to directly antagonize phytopathogens [17]. Importantly, interactions among microbes can further stimulate antibiotic synthesis, for instance, microbes like *Streptomyces* species can often respond to the presence of other microorganisms by upregulating their antibiotic production, effectively enhancing their biocontrol capabilities through reciprocal strategies [18, 19]. Collectively, these metabolites serve as communal resources, utilized by the entire community to support different biological processes and interactions, thereby maintaining microbiome stability and functionality [20–22]. Although metabolite-mediated microbial interactions have been extensively studied [23], the role of metabolites from native soil microbiomes and their effects on biocontrol agents remains relatively unexplored.

Among the myriad plant-associated microorganisms, *Streptomyces* species stand out for their exceptional production of bioactive metabolites, making them a valuable resource in agriculture due to their antifungal and antibacterial properties [24]. Notably, *Streptomyces* spp. play a crucial role in promoting plant health through the production of metabolites such as kakadumycin and coronamycins [25, 26], as well as the synthesis of phytohormones including indole-3-acetic acid (IAA) and abscisic acid (ABA), along with the enzymatic degradation of 1-aminocyclopropane-1-carboxylic acid (ACC) via ACC deaminases. These attributes make *Streptomyces* spp. significant contributors to plant health [27–29] and influence the structure and composition of rhizosphere microbial communities [30, 31].

Soil-borne diseases such as bacterial wilt caused by *Ralstonia solanacearum* have a significant global impact on crop yield and quality, resulting in substantial economic losses and raising considerable food safety concerns [32]. While *Streptomyces* spp. are effective in disease control [33], it remains unclear whether the rhizosphere microbiome contributes to synergistic disease inhibition alongside *Streptomyces* spp. Our previous research demonstrated that the rhizosphere of healthy tomato plants exhibits a higher abundance of *Streptomyces* spp. compared to those infected with bacterial wilt disease, indicating the recruitment of *Streptomyces* spp. by tomatoes to establish a protective rhizosphere microbiome against this disease [34]. However, the exact mechanisms underlying the interactions between *Streptomyces* and indigenous soil microbes in contributing to plant disease suppression remain elusive.

In this study, we used *Ralstonia solanacearum* QL-Rs1115 (Rs1115) as the model pathogen and investigated the interactions within rhizosphere microbiomes between *Streptomyces* and other microorganisms, to elucidate their collective impact on the effectiveness of *Streptomyces* in plant protection. To simulate the natural environment of the rhizosphere microbiome, we constructed a synthetic community (SynCom) comprising 100 representative bacterial species selected based on 16S rRNA sequences derived from 122 complete genomes isolated from the tomato rhizosphere. Each species was represented by a single strain. This SynCom encompassed the majority of high-abundance bacteria in the tomato rhizosphere, closely simulating its initial microbiome composition although simpler than the original rhizosphere microbiome [35]. We examined the protective capability of *Streptomyces* against invasion by Rs1115 on plants through a series of cultivation-inoculation experiments in the greenhouse, extensive in vitro

co-cultivation tests, and using transcriptomic and metabolomic approaches to characterize the molecular changes in *Streptomyces* induced by interactions with other microbes. Our hypothesis posited that disease suppression by *Streptomyces* spp. is influenced not only by their direct interactions with pathogens and plants through bioactive compound utilization but also by their interactions with other rhizosphere microbes. Therefore, our study aimed to uncover how *Streptomyces*' engagement with the soil microbiome impacts its protective efficacy against diseases, identify key soil microbes involved in this process, and elucidate the microbe-microbe interaction mechanisms within the rhizosphere. Our findings yield novel insights into how the rhizosphere microbiome enhances the biocontrol capabilities of *Streptomyces* spp., highlighting the cooperative interactions between *Streptomyces* spp. and native soil microbes for strengthening defenses against pathogenic invasions.

Results

Antagonistic effects in vitro do not explain the plant protection ability of *Streptomyces*

We initially screened various *Streptomyces* strains for their ability to control the pathogen Rs1115 in soil environments and facilitate the subsequent mechanistic investigations. To this end, we assessed 50 *Streptomyces* strains (detailed in Table S1, Fig. S1a, Fig. S2) for their capacity to control wilt disease. All strains exhibited antagonistic effects against Rs1115 on nutrient agar (NA) medium plates, with inhibition zone diameters ranging from 0.99 to 6.59 cm (Table S1) (This inhibition zone data were from Yang et al. [34]). Subsequently, we assessed their plant protection ability in natural soils through a greenhouse experiment. The biocontrol efficiency varied among the *Streptomyces* spp., ranging from 8.34% (strain R37) to 100% (strains R02, R21, R33, R35, and Y1), with an average efficiency of 58.71% (Table S1). To determine whether direct inhibition was the primary mechanism of disease suppression, we analyzed the association between laboratory-measured inhibition of Rs1115 (indicated by the diameter of the inhibition zone) and greenhouse-determined biocontrol efficiency of these *Streptomyces* spp. Surprisingly, no significant associations were discovered (Fig. 1a, $P = 0.82$, $R^2 < 0.01$, $F_{(1,48)} = 0.053$), suggesting that direct inhibitions by *Streptomyces* alone do not fully account for their protective effects on plants. This led us to hypothesize that the plant protection ability of *Streptomyces* spp. is determined by the interaction between *Streptomyces* spp. and the native rhizosphere microbiome. To validate this hypothesis, further investigation was conducted using twelve superior biocontrol efficient strains (efficiency range 68.76 to 100%) (Fig. S3, Table S1), which displayed varying vegetative and spore structures as well as physiological characteristics including temperature, pH, salinity tolerances, enzyme activities, and rhizosphere colonization abilities (Fig. S4, Table S2). Through these phenotypic, physiological, and biochemical analyses along with further averaged nucleotide identity (ANI) examinations, we found that strains R02 and R17 (ANI = 97.29%) belonged to the same species but were different strains. The remaining ten strains were identified as different *Streptomyces* species, with ANI values ranging from 84.09 to 90.77% (Table S3, Table S4), indicative of their diverse phylogenetic backgrounds and varying biocontrol potential.

Host protection ability of *Streptomyces* is linked to the rhizosphere microbiome

To simplify the intricate interactions within the natural rhizosphere soils of tomato plants, we constructed a synthetic community (SynCom) consisting of 100 well-characterized bacterial strains isolated from the tomato rhizosphere, representing the bacterial community in tomato rhizosphere soil (Table S5). We conducted greenhouse experiments in which we applied the twelve *Streptomyces* strains both individually in sterile substrate and in combination with the constructed SynCom to assess plant protection against the disease (Fig. S1b, c, Fig. S5, Fig. S6). We found that compared with the *Streptomyces* strains alone (with an average biocontrol efficiency of 48.73%), the combination of *Streptomyces* with SynCom significantly enhanced biocontrol efficiency (with an average biocontrol efficiency of 70.56%, Fig. 1b, $P = 0.0004$, df = 18.26, $t = -4.32$, two-sided Student's *t*-test). The pathogen density (defined as the abundance of *R. solanacearum*-specific *fliC* gene copy numbers per gram of dry soil, quantified by qPCR) in each treatment combining *Streptomyces* with SynCom was significantly lower than in treatments with SynCom or the pathogen alone (Fig. 1c, $P < 0.001$, $F_{(13,42)} = 283.3$, Dunnett-test). These results indicated that the co-application of *Streptomyces* and SynCom provides significantly greater plant protection than either the SynCom or individual *Streptomyces* strains alone, suggesting a synergistic biocontrol effect. In line with the natural soil, the correlation between the direct inhibition of the twelve *Streptomyces* strains (in the absence of the SynCom) and their biocontrol efficiency was not significant in the sterile substrate (Fig. S7, $P = 0.36$, $R^2 = 0.08$, $F_{(1,10)} = 0.92$). Similarly, there was no significant correlation between the direct inhibition of the twelve *Streptomyces* strains (with the presence of SynCom) and their biocontrol efficiency (Fig. 1d, $P = 0.26$, $R^2 = 0.04$, $F_{(1,10)} = 1.42$). Overall, direct inhibition by *Streptomyces* alone did not sufficiently predict their plant protection potential, and the presence of SynCom members enhanced the biocontrol effect of *Streptomyces* spp.,

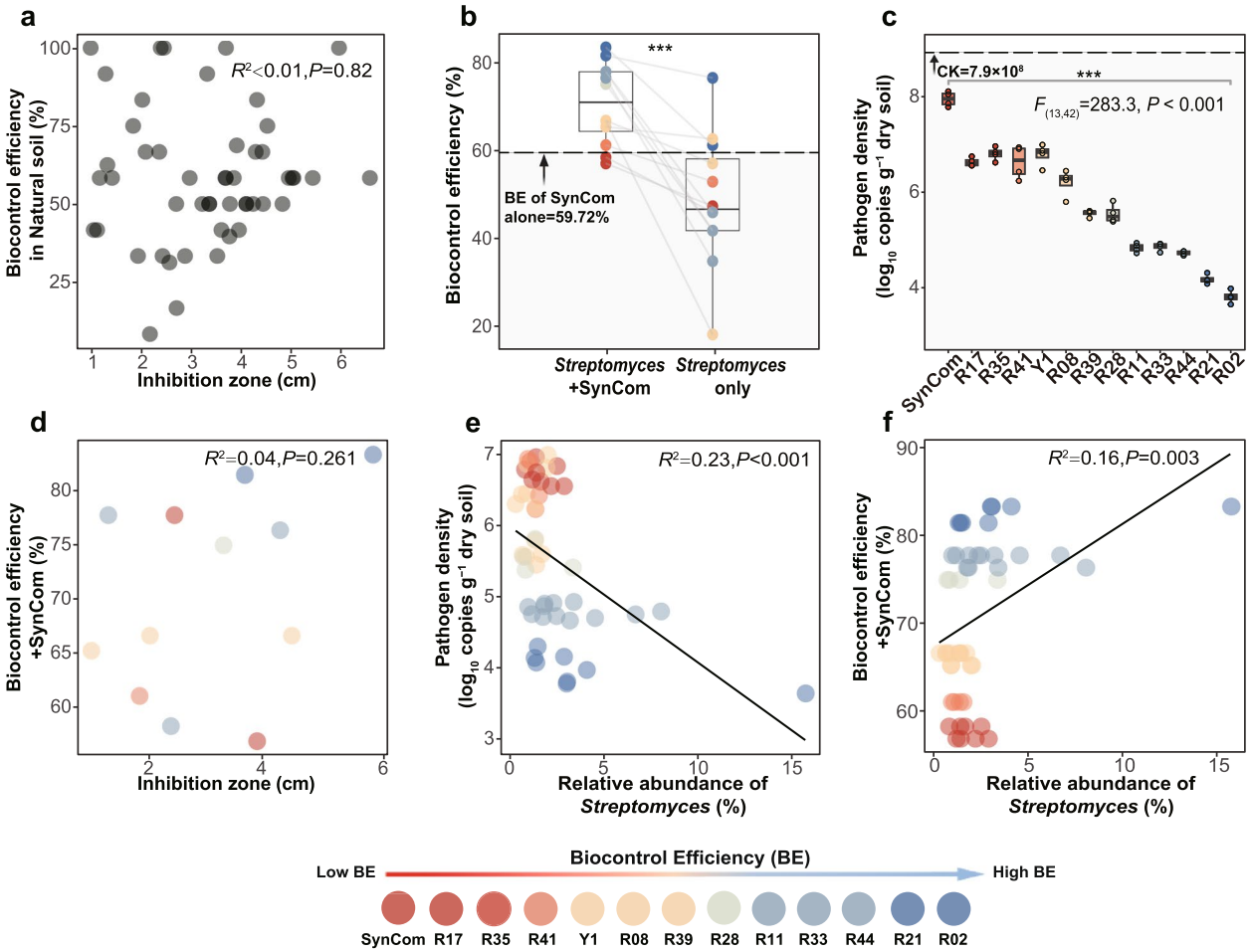

Fig. 1 Antagonistic effect of *Streptomyces* against the pathogen and impact of rhizosphere microbes on biocontrol efficiency. **a** Correlation analysis between the direct pathogen inhibition capacity of 50 *Streptomyces* isolates (as indicated by the average diameter of the inhibition zone) and their biocontrol effectiveness in natural soil. **b** Comparison of biocontrol efficiency between individual applications of *Streptomyces* and its use within a synthetic community (SynCom); the shaded area highlights the biocontrol efficiency attributable to SynCom alone (biocontrol efficiency of SynCom = 59.72%). **c** Box plots depicting the pathogen density in each treatment (RXX/Y1: various *Streptomyces* combinations with SynCom against Rs1115; SynCom: inoculated only with the synthetic community). The shaded area shows the pathogen density in the control treatment (CK) where Rs1115 was present alone (pathogen density in CK = 7.9×10^8 $\log_{10}$ copies g^{-1} dry soil). **d** Correlation analysis of direct pathogen inhibition and biocontrol efficiency for twelve *Streptomyces* isolates in combination with SynCom. **e** Significant correlation observed between *Streptomyces* relative abundance and pathogen density in a greenhouse experiment involving *Streptomyces* combined with SynCom. **f** Correlation analysis between the relative abundance of *Streptomyces* and its biocontrol effectiveness in the same experiment. The different colors of the nodes (from red to blue) represent low to high biocontrol efficiency for each treatment. Linear regression was fitted using the lm function

potentially due to synergistic interactions. These findings suggest that the disease suppression capabilities of *Streptomyces* are significantly influenced by the rhizosphere microbiome.

Inoculation of *Streptomyces* spp. promoted specific SynCom members in the rhizosphere

To investigate the impact of *Streptomyces* inoculations on the SynCom compositional dynamics and their implications for plant protection, we analyzed the bacterial communities in the tomato rhizosphere within a greenhouse experiment. This experiment paired each of the twelve *Streptomyces* strains with the SynCom to combat wilt disease (Table S6). By aligning 16S rRNA sequences from amplicon sequencing to those of SynCom strains from whole-genome sequencing, we detected all twelve *Streptomyces* strains in the tomato rhizosphere. The relative abundance of *Streptomyces* spp. was negatively correlated with pathogen density (Fig. 1e, $P < 0.001$, $R^2 = 0.23$, $F_{(1,46)} = 15.22$), and positively correlated with the biocontrol efficiency of *Streptomyces* on tomato plants (Fig. 1f, $P = 0.003$, $R^2 = 0.16$, $F_{(1,46)} = 9.85$). No impacts

on SynCom alpha diversity were observed ($P > 0.05$, Dunnett-test, TableS7). However, SynCom community composition was significantly affected by the *Streptomyces* spp., explaining 41% of community variations (Fig. 2a, $P < 0.001$, $R^2 = 0.41$, PERMANOVA).

We also observed that the SynCom with high biocontrol efficiency clustered at the top of the PCoA plot (Fig. 2a). Horizontal (PCoA1) and vertical (PCoA2) coordinates for each point were extracted to assess their correlations with *Streptomyces* biocontrol effects (Table S7). The results showed no significant associations between PCoA1 and the pathogen density ($P = 0.14$, $R^2 = 0.02$, $F_{(1,50)} = 2.23$) or biocontrol efficiency ($P = 0.056$, $R^2 = 0.05$, $F_{(1,50)} = 3.827$). However, PCoA2 significantly correlated with the pathogen density (Fig. 2b, $P = 0.004$, $R^2 = 0.134$, $F_{(1,50)} = 8.88$) and biocontrol efficiency of different *Streptomyces* treatments (Fig. 2c, $P = 0.004$, $R^2 = 0.14$, $F_{(1,50)} = 9.164$), suggesting that the protection ability of *Streptomyces* spp. on plants is associated with the SynCom structure. Additionally, we used the pairwise DESeq analysis and Upset plots to analyze the commonly shared enriched SynCom members across *Streptomyces* treatments. Among these shared species, the SynCom member CSC98 (*Stenotrophomonas maltophilia*) was the most commonly shared across *Streptomyces* spp. with high biocontrol efficiency (Fig. 2d, Fig. S8).

S. maltophilia CSC98 and *P. cellulositrophicus* CSC13as keystone taxa

To further investigate the interactions between SynCom members and *Streptomyces* species, we conducted the co-occurrence network analysis of the rhizosphere microbiome using the Molecular Ecological Network Analysis (MENA) pipeline and visualized the results with Gephi (Fig. 3a, Table S8, S9). The network comprised 518 positive and 116 negative correlations. Among these, 21 correlations were observed between SynCom members and *Streptomyces*, as well as 16 correlations between

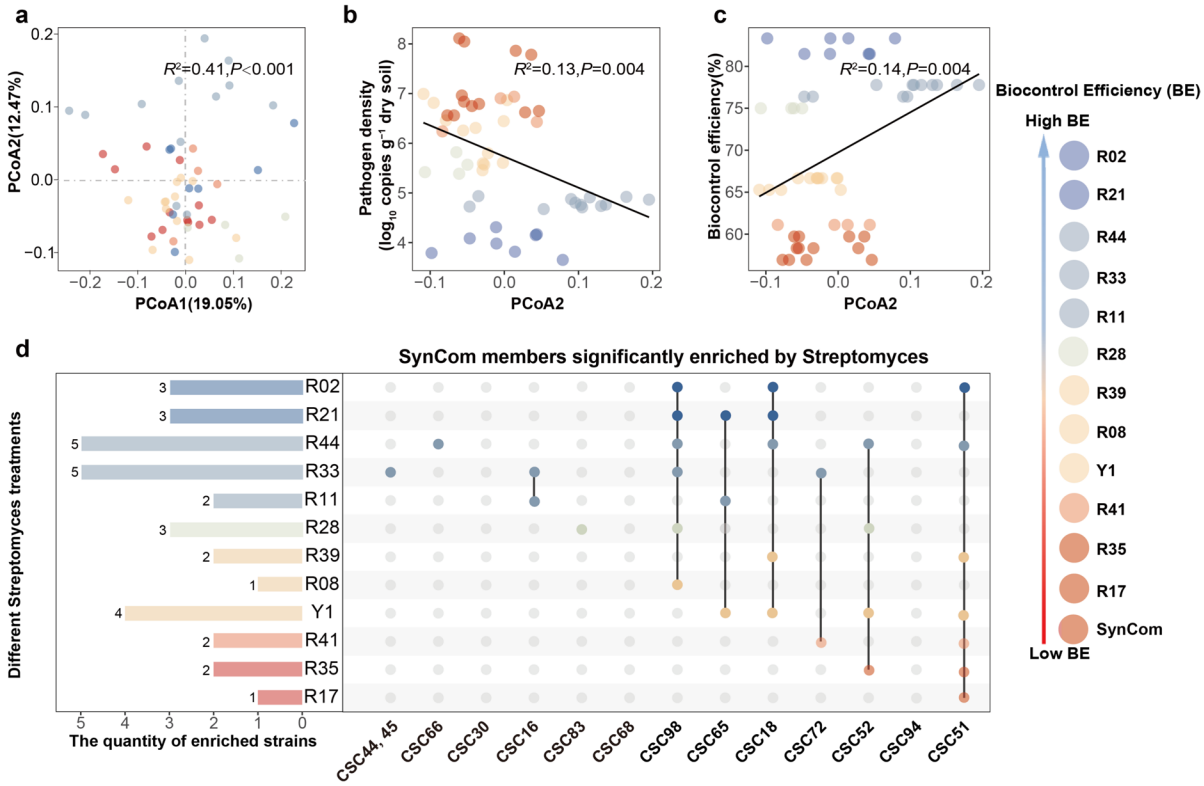

Fig. 2 Impact of *Streptomyces* on community diversity in greenhouse experiments. **a** Principal coordinate analysis (PCoA) with Bray-Curtis dissimilarity showing the community structure when combining *Streptomyces* with SynCom. Significant differences in microbiome community structures were observed among various *Streptomyces* treatments, with the structure of the bacterial community distinctly separated along the PCoA2 axis. The PCoA1 and PCoA2 values for each isolate were extracted to demonstrate changes in microbiome structure under different *Streptomyces* spp. treatments based on biocontrol efficiency, with each point colored according to biocontrol efficiency. **b** Relationship between PCoA2 and pathogen density, with the black line representing the linear regressions and 95% confidence intervals ($n = 52$, $P = 0.004$). **c** Correlation analysis between PCoA2 and biocontrol efficiency, illustrated by linear regressions with 95% confidence intervals ($n = 52$, $P = 0.004$). **d** UpSet plots showing all significantly enriched bacterial species in SynCom; CSC98 (*Stenotrophomonas* sp.) was particularly prevalent in treatments with high biocontrol efficiency (blue). All linear regressions were performed using the lm function

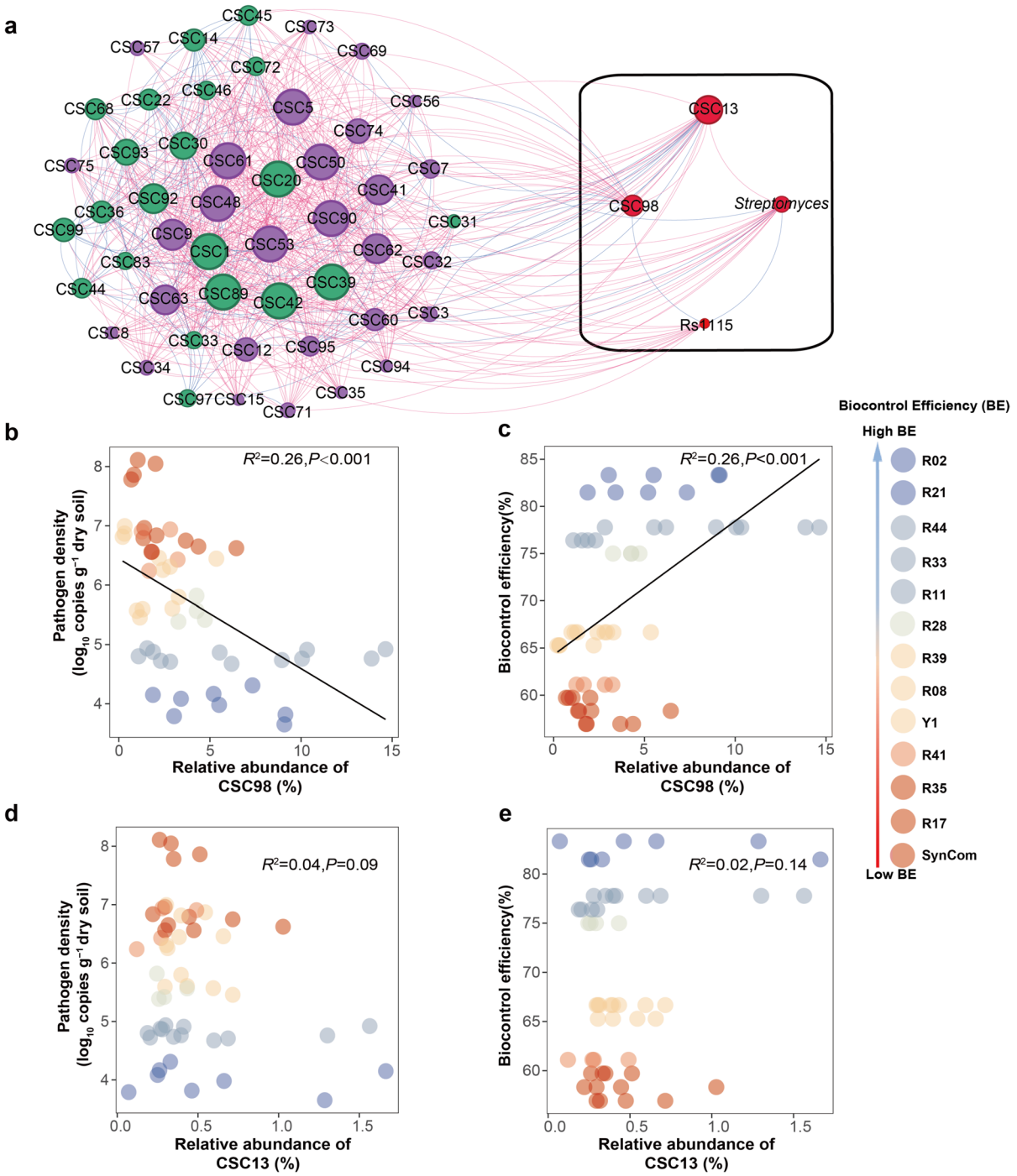

Fig. 3 An integrated analysis of microbial community interactions between *Streptomyces* and SynCom, highlighting their impact on biocontrol efficiency. **a** Co-occurrence network analysis for rhizosphere samples from 12 *Streptomyces* strains and SynCom, showing specific interactions, particularly between CSC13, *Streptomyces*, and CSC98. The node of *Streptomyces* represents 12 strains of *Streptomyces*. Nodes are color-coded by module (green and purple) and sized by their network degree (target members in red). Red edges denote synergistic interactions, while blue edges indicate antagonistic effects. **b** Correlation analysis between the relative abundance of CSC98 and pathogen density, with a black line showing linear regression and 95% confidence intervals ($n = 52$, $P < 0.001$). **c** Analysis of the correlation between the relative abundance of CSC98 and biocontrol efficiency, with regression lines as described ($n = 52$, $P < 0.001$). **d** Correlation analysis between the relative abundance of CSC13 and pathogen density. **e** Analysis of the correlation between the relative abundance of CSC13 and biocontrol efficiency. Each point was color-coded to indicate pathogen suppression efficiency. The different colors of the nodes (from red to blue) represent low to high biocontrol efficiency (BE) for each treatment. All regressions were fitted using the lm function

SynCom members and the pathogen Rs1115. Notably, both CSC98 and CSC13 exhibited strong connections with *Streptomyces* and Rs1115, suggesting their potential roles as keystone taxa in aiding *Streptomyces* spp. in controlling the pathogen (Fig. 3a). Among the relationships, strain CSC98 was directly associated with Rs1115 and indirectly associated with *Streptomyces* via CSC13. Subsequently, we found that CSC98 had a significant positive correlation with the plant protection ability (Fig. 3b, $P < 0.001$, $R^2 = 0.26$, $F_{(1,50)} = 18.68$ for pathogen density and Fig. 3c, $P < 0.001$, $R^2 = 0.26$, $F_{(1,50)} = 19.37$ for biocontrol efficiency), while CSC13 did not significantly correlate with either pathogen density (Fig. 3d, $P = 0.09$, $R^2 = 0.37$, $F_{(1,50)} = 2.97$) or the biocontrol efficiency (Fig. 3e, $P = 0.14$, $R^2 = 0.02$, $F_{(1,50)} = 2.19$). These findings suggest that CSC98 has a direct role in the suppression of Rs1115, and CSC13 acts as a mediator in the *Streptomyces*' interactions with CSC98.

Synergistic effects of keystone taxa and *Streptomyces* inhibit the pathogen

To investigate how interactions between *Streptomyces* R02, which exhibited the most effective biocontrol against Rs1115, and the key SynCom species (*S. maltophilia* CSC98 and *P. cellulositrophicus* CSC13) influence the biocontrol efficiency against Rs1115, we conducted multiple cross-feeding experiments using metabolites from the supernatants of liquid culture of the strains (Fig. S1 d). Our results showed that the supernatant containing metabolites from *Streptomyces* R02 significantly promoted the growth of CSC13 (Fig. 4a, $P < 0.001$, df = 21.97, $t = 4.27$, two-sided Student's *t*-test), while it had no effects on the growth of CSC98 (Fig. 4b, $P = 0.67$, df = 16.83, $t = 0.44$, two-sided Student's *t*-test). Furthermore, metabolites from CSC98 significantly promoted the growth of CSC13 (Fig. 4c, $P < 0.001$, df = 21.65, $t = 5.76$, two-sided Student's *t*-test). Similarly, the metabolites from CSC13 also significantly promoted the growth of CSC98 (Fig. 4d, $P = 0.0041$, df = 19.16, $t = 3.26$, two-sided Student's *t*-test). These findings demonstrated a mutually beneficial relationship among *S. maltophilia* CSC98, *Streptomyces* R02, and *P. cellulositrophicus* CSC13, suggesting synergistically metabolic interactions that contribute to the collective biocontrol efficacy of *Streptomyces* R02 against Rs1115.

We then investigated the antagonisms between the two keystone microbes, *Streptomyces* R02 and the pathogen, by focusing on direct inhibitory effects and nutritional competition. These bacterial strains had distinct colony morphologies: yellowish pink for the pathogen, golden yellow for CSC98, and pale for CSC13, which aided colony counting to assess competition in co-cultivation experiments. Our results showed that CSC98 strongly competed with Rs1115 for nutrients and significantly inhibited the growth of Rs1115 (Fig. 4e, $P < 0.001$, $F_{(3,12)} = 196.40$, ANOVA). In contrast, strain CSC13 did not compete nutritionally with Rs1115 (Fig. 4f, $P < 0.001$, $F_{(3,12)} = 384.70$, ANOVA), but promoted the growth of *Streptomyces* R02 (Fig. 4g, $P < 0.001$, $F_{(2,33)} = 386.10$, ANOVA). The supernatant of *S. maltophilia* CSC98 and *P. cellulositrophicus* CSC13 alone did not inhibit Rs1115. Furthermore, neither the co-cultured supernatants of the two strains nor an equal mixture of their supernatants affected Rs1115 (Fig. 4h, $P = 0.29$, $F_{(6,77)} = 1.25$, Dunnett-test). This is consistent with the result that CSC13 and CSC98 did not directly interact (e.g., inhibit) with Rs1115 on NA plates (Fig. S9). Interestingly, as shown in our cross-feeding experiments, the supernatant of CSC98 and CSC13 significantly enhanced the inhibitory effect of *Streptomyces* R02's supernatant on Rs1115, with the supernatant from CSC13 showing the strongest enhancement among all treatments (Fig. 4i). Different combinations/orders of supernatant treatments also influenced the biocontrol efficiency of R02 (Fig. 4i). In the CSC98_CSC13 + R02 treatment, where the CSC13 was first treated with the supernatant of CSC98, followed by treating R02 with the supernatant of CSC13, we observed significant higher inhibition of Rs1115 ($P < 0.001$) than R02 alone. In the reverse order treatment, where CSC98 was treated with the supernatant from CSC13 before R02 received the CSC98 supernatant, a similar inhibition level of Rs1115 ($P < 0.001$) was observed than R02 alone (Fig. 4i). In the co-culture treatment (co-culture + R02), where R02 was treated with the supernatant from the co-culture of CSC98 and CSC13, we observed a significant reduction in Rs1115 turbidity compared to the control (Rs only), but the inhibition was less pronounced than in the sequential treatments (CSC98_CSC13 + R02, CSC13_CSC98 + R02, CSC13 + R02, and CSC98 + R02). Notably, for cross-feeding experiments, bacterial cultures were standardized by diluting cultures to an OD_{600} of 0.5 using a SpectraMax M5 plate reader, followed by centrifugation (7000 rpm, 10 min, 4℃) and filter sterilization (Millex-GP Filter, 0.22 μm, PES membrane, SLGPR33RB) to remove living cells. Overall, these results highlight the importance of the specific bacterial interactions in maximizing antagonistic activity, and these inhibitory effects appear to be driven by microbial interactions and enhanced antimicrobial production of R02 by CSC13 rather than by increased biomass of *Streptomyces* R02 (Fig. 4i, $P < 0.001$, $F_{(7,88)} = 215$, Dunnett-test and Tukey's multiple range) (Table S10).

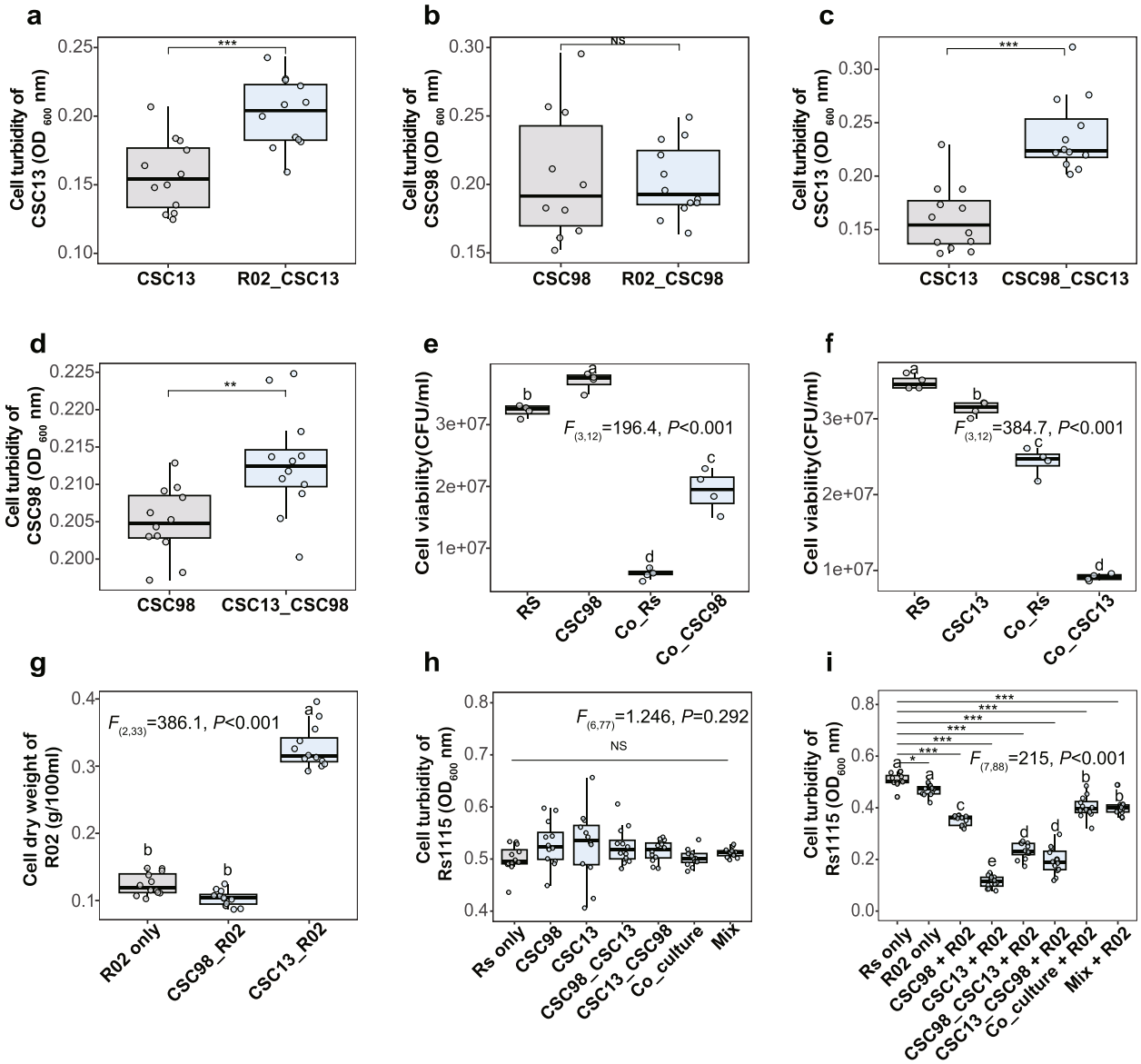

Fig. 4 Quantitative analyses of microbial growth characteristics and interactions for *Streptomyces* R02, pathogen Rs1115, and strains CSC98 and CSC13. **a** Box plots comparing the impact of *Streptomyces* R02 supernatant on strain CSC13's growth. **b** Box plots showing the influence of *Streptomyces* R02 supernatant on strain CSC98's growth. **c** Box plots illustrating the effect of CSC98 supernatant on CSC13's growth. **d** Impact of CSC13 supernatant on CSC98's growth. **e** Co-culture of strain CSC98 with Rs1115. **f** Co-culture of strain CSC13 with Rs1115. **g** Effects of supernatants from strains CSC98 and CSC13 on the growth of *Streptomyces* R02. **h** Impact of supernatants from various strains and their combinations (excluding *Streptomyces* R02) on Rs1115 growth. **i** Effects of single and combined bacterial supernatants on Rs1115's inhibition by *Streptomyces* R02 supernatant. Legend: R02_CSCXX indicates strain CSCXX treated with *Streptomyces* R02 supernatant. CSCXX_R02 indicates the biomass of *Streptomyces* R02 treated with strain CSCXX's supernatant. CSCXX represents strain CSCXX alone. CSCAA_CSCBB shows strain CSCBB treated with strain CSCAA supernatant. RS indicates the growth of Rs1115 alone. Co_RS (**e**) and Co_RS (**f**) refer to Rs1115 in co-culture systems with strains CSC98 and CSC13, respectively. Co_CSCXX indicates strain CSCXX in co-culture with Rs1115. R02 only (**g**) represents the biomass of *Streptomyces* R02 alone. Rs only (**h**, **i**) represents OD_{600} nm of Rs1115 alone. R02 only (**i**) represents OD_{600} nm of Rs1115 treated with strain R02 supernatant. Co_culture (**h**, **i**) represents the co-culture of strains CSC13 and CSC98. Mix (**h, i**) denotes supernatant from mixed strains CSC13 and CSC98 in equal proportions

Transcriptomic and metabolomic analysis of the biocontrol efficiency

Our results revealed a promoted inhibitory effect of *Streptomyces* R02 on Rs1115 when the *Streptomyces* was influenced by metabolites from CSC13, as observed in the glasshouse and cross-feeding experiments. To

elucidate the mechanisms, we investigated the transcriptional and metabolic changes in *Streptomyces* R02 cells with and without CSC13 metabolites (Fig. 5). There were significant differences in the gene expressions ($P = 0.005$) (Fig. 5a**,** Fig. S10a) with 1915 differentially expressed genes between R02 and CSC13_R02 treatments (7 days post-inoculation in NB medium) (Table S11, Fig. S10a, b). Major transcriptional changes were associated with 19 different pathways, including oxidative phosphorylation, valine, leucine, and isoleucine degradation (Fig. 5b, Fig. S10c, Table S12), indicating that CSC13 induced significant metabolic alterations in *Streptomyces* R02.

Importantly, the CSC13 + R02-treated group showed a substantial increase in the antibacterial secondary metabolite Erythromycin E ($P < 0.001$, $F_{(2,15)} = 234$) compared to the R02 only and CSC13 only groups, which both showed a low abundance of the compound (Fig. 5). In details, metabolomics of CSC13 + R02, CSC13 only, and R02 only revealed a total of 6896 metabolites, comprising 33.74% amino acids and derivatives, 10.80% organic acids, 10.34% glycerophospholipids (GP), 5.28% alkaloids, and 11.28% others including ketones, aldehydes, lactones, and saccharides (Fig.S11a, Table S13). Cluster heatmap analysis revealed significant differences in the metabolite production across the three groups (R02 only, CSC13 only, and CSC13 + R02), which were distributed into eight clusters. Metabolites in clusters 1 and 2 were most abundant in the CSC13-only group, while clusters 3, 5, and 7 peaked in the R02-only group. Conversely, clusters 4, 6, and 8 showed the highest levels in the CSC13 + R02 group (Fig. S11b). The biological replicates clustered closely, indicating high homogeneity among them, and the PCoA analysis revealed significant differences between the groups (Fig. 5c, explaining 62% of variance, $P = 0.001$). The differential metabolite analysis between the CSC13 + R02 and R02 only groups revealed significantly enriched metabolites in the CSC13 + R02 group, which were mainly amino acids and derivatives, benzene and substituted derivatives, lactones, and so on (Fig. 5d, Table S14) and significantly enriched metabolites in pathways including (i) the biosynthesis of secondary metabolites, (ii) the biosynthesis of antibiotics, and (iii) other related metabolic pathways (Fig. S11c, d, e).

The CSC13-induced key genes were linked to the metabolites in *Streptomyces* R02, collectively contributing to the enhanced inhibition of Rs1115. We identified 30 key genes that were upregulated in expression in *Streptomyces* R02 treated with CSC13's metabolites, which were all significantly associated with the production of the antibacterial compound Erythromycin E (Fig. 5e, S12). These genes were from five major transcriptomic pathways in *Streptomyces*: (i) valine, leucine, and isoleucine degradation; (ii) glycolysis/gluconeogenesis; (iii) inositol phosphate metabolism; (iv) phenylalanine metabolism; and (v) geraniol degradation and biosynthesis of secondary metabolites (Fig. 5e, S12). Through validation experiments with the key compound Erythromycin E, we confirmed its strong inhibitory against Rs1115. The diameter of the inhibition zone of Erythromycin E against Rs1115 ranged from 3.5 ± 0.043 to 0.84 ± 0.026 cm (Fig. 6a), with a minimum inhibitory concentration (MIC) was 0.25 μg/mL (Fig. 6b, Table S15). As the concentration of Erythromycin E decreased from 256 to 0.25 μg/mL, both the diameter of the inhibition zone and the inhibition of Rs1115 cells in liquid culture decreased significantly (Fig. 6c, d). Overall, the results from transcriptomic, metabolomic, and validation analyses provide strong evidence that CSC13's metabolites significantly enhanced *Streptomyces* R02's ability to inhibit Rs1115 (Fig. 7).

Discussion

Our study found that the in vitro antagonistic effects of *Streptomyces* did not explain their ability to protect tomato plants from the pathogen Rs1115 in natural soils. Greenhouse experiments showed significant variability in biocontrol efficiency among 50 *Streptomyces* strains, but no correlation between in vitro inhibition and plant protection was observed. We found that combining

(See figure on next page.)

Fig. 5 Transcriptomic and metabolomic analysis of *Streptomyces* R02 under *Paenibacillus cellulositrophicus* CSC13 treatment (using supernatant metabolites). **a** Two-dimensional principal coordinate analysis (PCoA) of Bray-Curtis dissimilarity comparing the transcriptome of *Streptomyces* R02 with the co-culture of *Streptomyces* R02 and *P. cellulositrophicus* CSC13's metabolites (71% of variance explained, $P = 0.005$, $n = 12$). **b** Bubble plot showing significantly enriched key genes from the KEGG enrichment analysis. Major transcriptional changes were observed in genes associated with pathways of (i) valine, leucine, and isoleucine degradation, (ii) glycolysis/gluconeogenesis, (iii) inositol phosphate metabolism, (iv) phenylalanine metabolism, and (v) geraniol degradation and secondary metabolite biosynthesis, which are highlighted in red. **c** PCoA illustrating significant differences in metabolite compositions between *Streptomyces* R02 only, *P. cellulositrophicus* CSC13 only, and co-culture of *Streptomyces* R02 and *P. cellulositrophicus* CSC13's metabolites (CSC13 + R02) (62% of variance explained, $P = 0.001$, $n = 18$). **d** Bubble plot showing enriched metabolites in the R02 + CSC13 treatment group compared with the R02-only control. The pathway containing the key metabolite, Erythromycin E, is highlighted in red (Lactones). **e** Mantel test demonstrating significant correlations between the metabolite Erythromycin E and key genes, and the inset graph showed the structure and abundance of Erythromycin E under different conditions

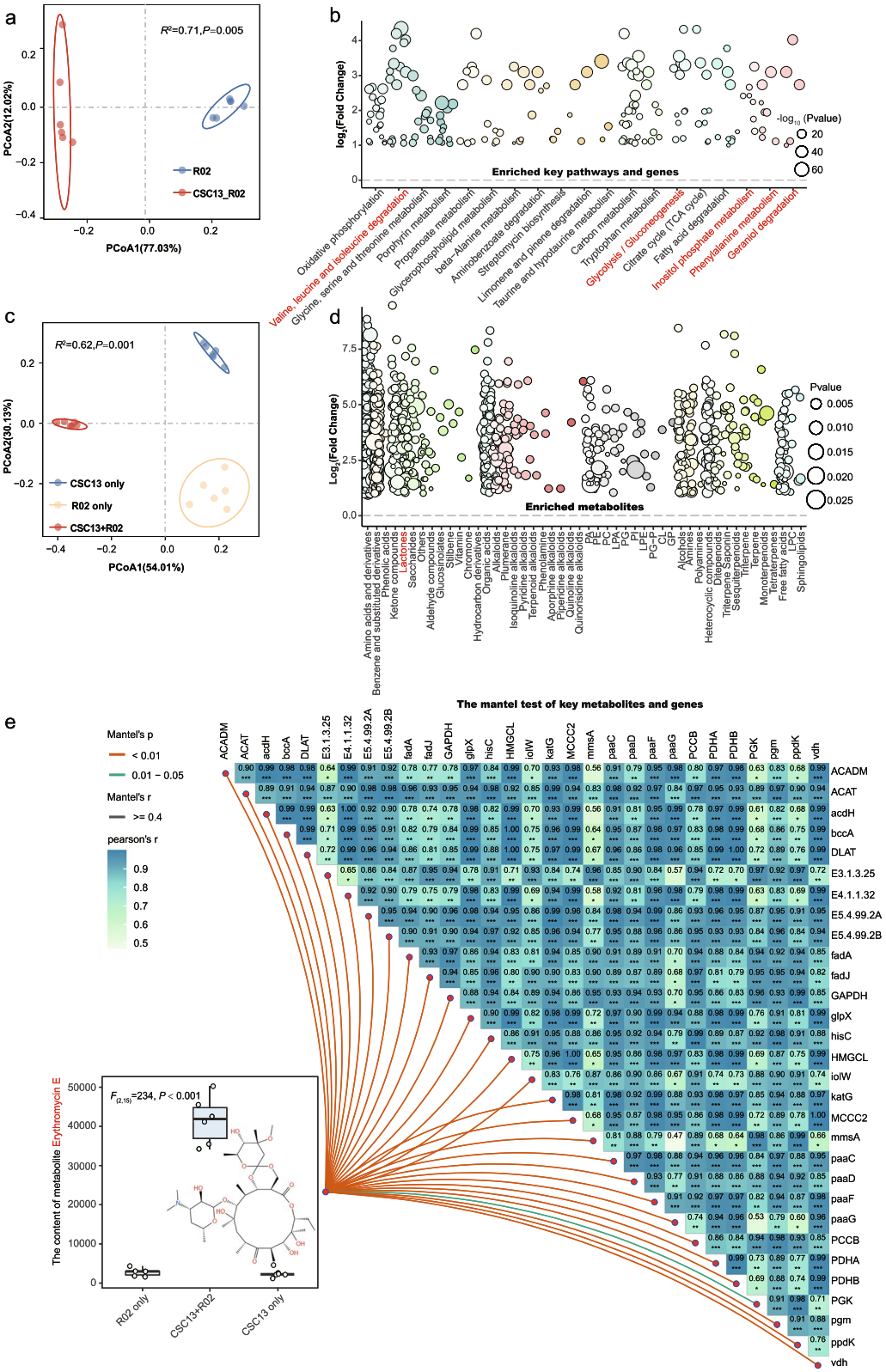

Fig. 5 (See legend on previous page.)

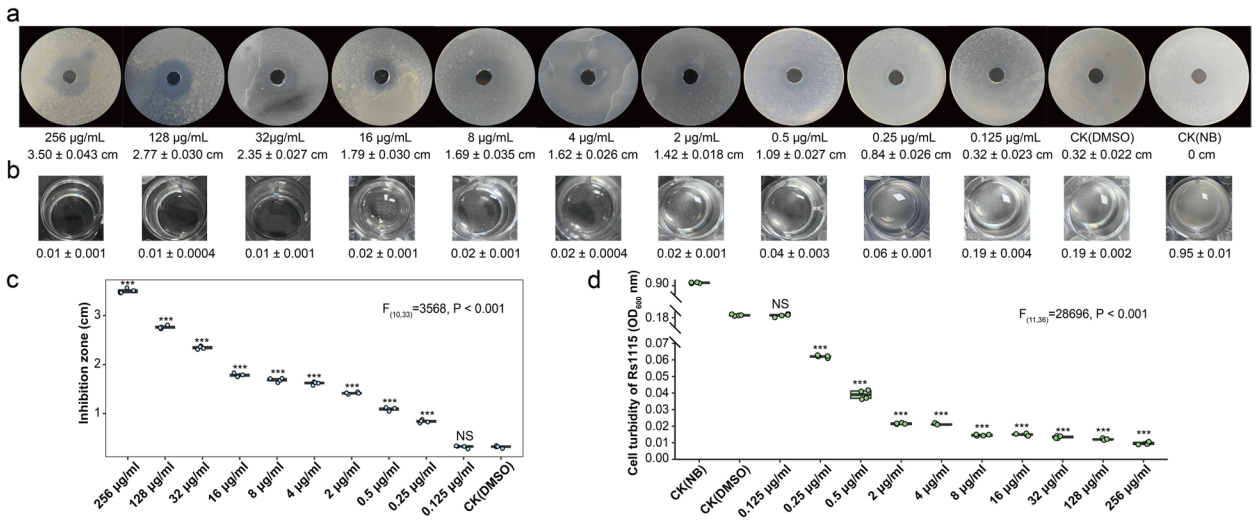

Fig. 6 The inhibition effect of Erythromycin E against Rs1115. **a** Images of agar diffusion assays showing the inhibition zones of Rs1115 in response to different concentrations of Erythromycin E. The compound was applied in a gradient from 0.125 to 256 μg/mL, with negative controls CK (nutrient broth medium) and CK (dimethyl sulfoxide, DMSO). The mean diameters of inhibition zones (± standard error) are indicated below each corresponding plate. **b** Images of bacterial growth in liquid NB medium supplemented with different concentrations of Erythromycin E. Optical density (OD_{600}) measurements are provided, showing bacterial turbidity at 24 h post-incubation. **c** Quantification of inhibition zones from the agar diffusion assay. **d** Growth inhibition of Rs1115 in liquid culture, as determined by OD_{600} measurements after 24 h of incubation with different concentrations of Erythromycin E. Statistical significance in these graphs is indicated (****P* < 0.001; NS, not significant)

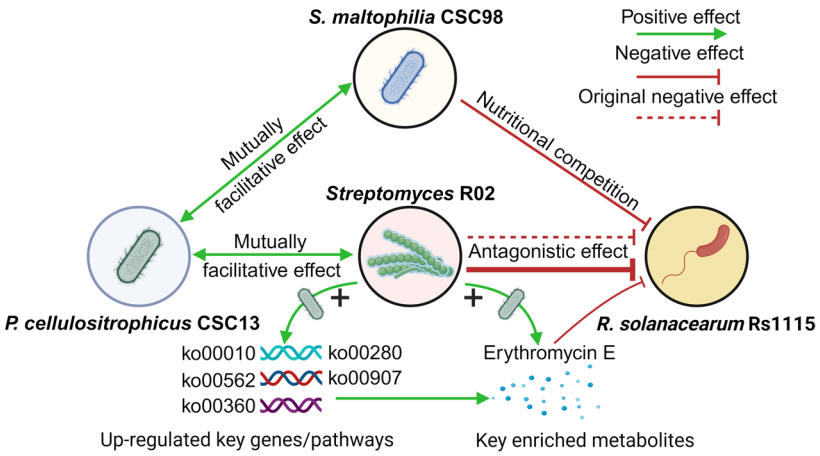

Fig. 7 The diagram illustrates the enhanced inhibition of *Streptomyces* R02 on *Ralstonia solanacearum* Rs1115 through interactions with *Stenotrophomonas maltophilia* CSC98 and *Paenibacillus cellulositrophicus* CSC13 in soil. *S. maltophilia* CSC98 and *P. cellulositrophicus* CSC13 demonstrated a mutually facilitative relationship, where each species promoted the growth and/or activity of the other. Similarly, *P. cellulositrophicus* CSC13 and *Streptomyces* R02 also exhibited mutual facilitation, with both species benefiting from their interaction. Under this facilitation, *Streptomyces* R02 exhibited stronger inhibition of *R. solanacearum* Rs1115, compared to when CSC13 was absent. This inhibition was attributed to the CSC13-induced production of bioactive secondary metabolites in *Streptomyces* R02, Erythromycin E, which we confirmed to directly inhibit *R. solanacearum* on nutrient agar and in nutrient broth. The induction of Erythromycin E in *Streptomyces* R02 by CSC13 was associated with the upregulation of key genes across five major genetic pathways. In contrast, *S. maltophilia* CSC98 and *R. solanacearum* Rs1115 displayed nutritional competition, resulting in a negative interaction likely due to competition for shared resources and limiting their growth potential. The microbial interaction model reveals the critical role of *Streptomyces* R02 and its interactions with two bacterial strains in controlling against a major plant pathogen, mediated by upregulations of key genes and a metabolite in the *Streptomyces*

Streptomyces spp. with a simulated rhizosphere microbiome, significantly enhanced plant protection, suggesting that microbial interactions in the rhizosphere play a critical role in pathogen inhibition. In particular, two SynCom species, *S. maltophilia* CSC98 and *P. cellulositrophicus* CSC13, emerged as keystone taxa [36], enhancing

biocontrol efficiency through synergistic interactions with *Streptomyces* R02. Metabolite analysis revealed that the antibiotic Erythromycin E was notably upregulated by CSC13 metabolites and showed a significant increase among enriched metabolites (other compounds, such as paromomycin, were also enriched, however, significant genetic changes associated with its biosynthesis have not yet been identified in this study (Fig. S13)). Although CSC13 also largely promoted R02 growth (by +2.64 folds), the substantial increase in Erythromycin E (by +14.93 folds) indicates its primary role as a metabolic inducer activating antibiotic biosynthesis pathways (Fig. S12). Overall, our findings suggest that the protective effect of *Streptomyces* on plants extends beyond direct interactions with the pathogen to include synergies with the rhizosphere microbiome, highlighting the importance of microbial interactions in natural soils for effective biocontrol.

Streptomyces spp. are effective biocontrol agents against a wide range of plant pathogens, often utilizing antibiotic compounds and signaling metabolites [37, 38]. For instance, polyene antibiotics like amphotericin B target ergosterols—a key component of fungal cell membranes—destabilizing their membranes and causing oxidative damage. These antibiotics are effective against pathogenic fungi, such as *Fusarium* spp. [37, 38]. However, our results indicate that evaluating the biocontrol potential of *Streptomyces* spp. exclusively through in vitro agar plate assays significantly underestimates their actual protective capacity in plants, as these assays do not reflect complex microbial interactions occurring in soil microbiomes, which are also influenced by soil properties and climatic conditions. Our findings demonstrate that considering microbial interactions within the rhizosphere microbiome is essential, as these interactions greatly enhance the protective efficacy of *Streptomyces* spp. against Rs1115. The production of metabolites by one microbe that can stimulate the growth of another is a well-recognized phenomenon in microbial communities, playing a key role in sustaining cooperative networks within microbiomes [39]. This aligns with the mutual growth promotion observed between CSC98, CSC13, and *Streptomyces* R02 in our study. We observed a gradual decline in *Streptomyces* R02 colonization over time, possibly due to decreasing spore viability and adaptation to the stabilizing rhizosphere environment, indicating an initial transient colonization phase followed by microbial community equilibrium [40].

Metabolites from CSC13 significantly stimulated the production of Erythromycin E in *Streptomyces* R02, suggesting that the induction of specialized metabolites enhanced its biocontrol efficacy. Erythromycin E, a widely used macrolide antibiotic, exhibits potent antibacterial activity against both gram-negative and gram-positive bacteria [41]. Its production likely aided *Streptomyces* R02 in suppressing Rs1115. In agricultural systems, Erythromycin has strong antagonistic effects against bacterial pathogens, including *R. solanacearum*, contributing significantly to plant health [42]. While the above studies provide historical context for the antibiotic activity of erythromycin, they may not fully capture its role in plant protection against pathogens in current contexts. Our study addressed this gap by demonstrating, through dose-dependent inhibition assays (Fig. 6), that purified Erythromycin E from *Streptomyces* R02 effectively suppressed *R. solanacearum* even at low concentrations (with significant inhibition observed at just 0.25 μg/mL).

The mechanisms of the pathogen inhibition involved likely include Erythromycin exerting selective pressure on bacteria, thereby altering the composition of soil bacterial communities [43]. Previous studies have shown that Erythromycin can significantly increase the relative abundance of certain Proteobacteria and Firmicutes in soils, as some members of these groups may be Erythromycin-resistant and capable of utilizing it as a carbon and energy source [44, 45]. While these studies suggest that such effects typically occur at higher erythromycin concentrations, our observed concentrations fall within a lower yet still highly effective antimicrobial range against Rs1115. Consequently, the interaction between *Streptomyces* R02 and two key species-CSC13 (Firmicutes) and CSC98 (Proteobacteria)-remained unaffected by the increased production of Erythromycin E. Instead, it specifically reduced the abundance and activity of the pathogen Rs1115.

In vitro, *Streptomyces* R02's supernatant enhanced CSC13 growth (Fig. 4a) but not CSC98 (Fig. 4b). In contrast, rhizosphere data (Table S6) showed R02-boosted CSC98 abundance, not CSC13. These differences likely stem from simplified in vitro conditions versus the complex rhizosphere environment, influenced by nutrient availability, microbial competition, and plant interactions. CSC98 may have soil-specific advantages, while CSC13's laboratory growth promotion might be limited in natural conditions. In this regard, further research is needed to clarify these mechanisms.

Stenotrophomonas spp. are significant members of the SynCom and are well-recognized for their ubiquitous presence in the rhizosphere, root endosphere, and phyllosphere (e.g., on leaves), where they form close associations with host plants [46, 47]. These bacteria can become enriched in the *Arabidopsis* rhizosphere following infection by the downy mildew pathogen *Hyaloperonospora arabidopsis*. This enrichment mediates the legacy effect of a primarily infected downy mildew population,

conferring enhanced protection against the pathogen in subsequent plant populations growing in the same soil [48]. Similarly, *Stenotrophomonas* spp. became enriched in the wheat rhizosphere following plant infections by crown rot disease caused by *Fusarium pseudograminearum*, mitigating infection in subsequent plant cycles [49]. These *Stenotrophomonas* species can produce a range of extracellular enzymes, including chitinases, elastases, lipases, nucleases, and proteases [47, 50]. These enzymes play crucial roles not only for the bacteria themselves but also in facilitating the colonization of other rhizosphere microbes. They decompose plant cell-wall components and soil organic matter, enhancing nutrient availability for microbial proliferation and signaling [47]. Most *Stenotrophomonas* spp. also exhibit antifungal properties and mitigate fungal infections through iron competition [51]. These species can form biofilms in conjunction with other microbes, effectively colonizing the rhizosphere and enhancing the growth of various crops such as tomatoes, wheat, and lettuce [47]. In our study, *S. maltophilia* CSC98 inhibited Rs1115 through nutrient competition, likely due to its ability to deplete essential nutrients such as carbon, and nitrogen more efficiently, thereby starving Rs1115. Alternatively, it may produce siderophores like maltophores, which outcompete Rs1115's own siderophore systems and limit its access to iron.

Microbial interactions observed in the glasshouse and cross-feeding experiments highlight the pivotal role of *Stenotrophomonas* spp. in enhancing the growth of *Paenibacillus* sp. (CSC13). This enhancement is likely due to the ability of *Stenotrophomonas* spp. to produce extracellular substances such as enzymes and signaling compounds, which facilitate the breakdown of complex substrates into simpler nutrients that *Paenibacillus* can utilize. *Stenotrophomonas* may also produce growth-promoting hormones or substances like siderophores and phytohormones, indirectly benefiting *Paenibacillus* by improving its overall metabolism [47]. Similar to *Stenotrophomonas* spp., *Paenibacillus* spp. are predominantly found in plant and soil environments but have also been isolated from other habitats, such as the guts of honeybees infected by American foulbrood, where they act as pathogens [52]. When applied to plants, *Paenibacillus* spp. have demonstrated the ability to promote the growth of diverse crops, including maize, pumpkin, and rice [53–55]. Many strains of plant-associated *Paenibacillus* can produce indole- 3-acetic acid (IAA) and other auxin phytohormones [53–55]. Some strains also exhibit capabilities such as phosphate solubilization, atmospheric nitrogen fixation, and enhancement of plant iron uptake through the production of siderophores, such as bacillibactin produced by *Paenibacillus larvae* [52, 56, 57]. As discovered in this study, CSC13 significantly enhanced the inhibitory effect of *Streptomyces* R02 on Rs1115 by inducing the production of erythromycin E in *Streptomyces* R02. However, the specific metabolites produced by *Paenibacillus* sp. that triggered this production remain unidentified, warranting further investigations to dissect the interactions.

It remains uncertain whether this enhanced disease suppression by R02 is entirely due to direct antagonism or if plant immune responses, such as induced systemic resistance (ISR) [58], also play a role. It is plausible that Erythromycin E and other metabolites produced or enhanced by CSC13 contribute to ISR in tomato plants, aiding pathogen reduction. Analyzing immune-related gene expression in plants treated with R02 and its SynCom would clarify ISR's involvement. Additionally, using R02 mutants deficient in specific secondary metabolites, including Erythromycin E, could help distinguish between direct antagonism and ISR mechanisms underlying the observed biocontrol effects. As such, our results suggest that *Streptomyces* may enhance plant protection through at least two mechanisms. Firstly, the enhanced production of antimicrobial compounds, as demonstrated in co-culture with CSC13, contributes to pathogen suppression (Fig. 7). Secondly, R02 stimulated beneficial microbial populations, such as CSC98, which appears to suppress RS1115 growth through nutritional competition (Fig. 7). These dual contributions underline the complex ecological dynamics in the rhizosphere [1–3], which could be further explored in relation to the microbial interactions revealed in our study (Fig. 7).

The implications of our findings regarding the microbiome-induced enhancement of biocontrol efficiency in *Streptomyces* spp. are valuable for agricultural disease management strategies and the application of biocontrol agents in agroecosystems [59]. We presented a novel approach that leverages soil microbial interactions—particularly the synergistic effects driven by metabolic exchanges between microbes—to boost the biocontrol efficacy of *Streptomyces* spp. against plant pathogens. Biocontrol agents often fail to produce any effects in field conditions, mainly due to inadequate lab trials that do not take into consideration their associations with the native soil microbiota after applications. Moving beyond the traditional paradigm of direct microbial antagonisms [60], these findings provide alternative strategies for developing biocontrol consortia tailored to pathogens under various soil and environmental conditions, thereby fostering consistent and effective biocontrol effects in agricultural settings.

Conclusions

Our study revealed the importance of microbial interactions in enhancing the biocontrol efficacy of *Streptomyces* spp. against soil-borne pathogens like Rs1115. The integration of a SynCom from the rhizosphere demonstrated that the protective capabilities of *Streptomyces* spp. were significantly improved in cooperation with key rhizosphere microbes *S. maltophilia* CSC98 and *P. cellulositrophicus* CSC13. These interactions synergistically suppressed the pathogen Rs1115 through mechanisms that included the stimulated production of the crucial antibacterial compound Erythromycin E in *Streptomyces* R02 and nutrient competition with the pathogen. These findings highlight the necessity of considering complex microbial interactions within microbiomes, rather than relying solely on direct antagonism when developing effective biocontrol strategies. Future research should explore biocontrol agents and their metabolites under field conditions to advance the development of probiotics and postbiotics for agricultural applications.

Materials and methods

Microbes used in this study and their culturing conditions

In this study, we used *R. solanacearum* QL-Rs1115 (hereafter referred to as Rs1115, GenBank accession GU390462) as the model plant pathogen [61]. This Rs1115 strain was originally isolated from tomato plants in Qilin town, Nanjing, China (118° 57′ E, 32° 03′ N) and cultured overnight in nutrient broth medium (NB) (10.0 g glucose L^{-1}, 5.0 g peptone L^{-1}, 0.5 g yeast extract L^{-1}, and 3.0 g beef extract L^{-1}, pH 7.0; at 30℃, 170 rpm) for the subsequent inoculations. The pathogen cells were harvested by centrifugation (6000 rpm, 10 min), washed twice with sterile saline solution (0.9% NaCl), and diluted to a density of 10^7 colony forming units (CFU) mL^{-1} based on the optical density reading (OD_{600} = 0.5) before the experiments.

Among the *Streptomyces* strains used in this study, 48 strains (R01-R48) were isolated from the rhizosphere of wild-type tomato (*Solanum lycopersicum* cv. "Micro-Tom") [34], and two strains (Y1-Y2) were isolated from the tomato rhizosphere (*Lycopersicon esculentum* cv. "Red-Dwarf"), collected from Qilin Town, Nanjing, China (118°57'E, 32° 03'N). The microbial isolation method was previously described [34]. Briefly, the rhizosphere soil was suspended in sterile distilled water to form a soil suspension, which was serially diluted and spread on a Gauze's synthetic medium No. 1 agar plate supplemented with cycloheximide 50 mg L^{-1} and nalidixic acid 20 mg L^{-1} to suppress the growth of fungi and bacteria [62]. The growth of *Streptomyces* is relatively slow, and the plates were incubated at 28 °C for 15 to 20 days. Single colonies were then picked and transferred to an International *Streptomyces* Project medium 3 (ISP3) [63] for cultivation. Purified strains were preserved in glycerol (20%, v/v) at −80℃. The *Streptomyces* spores grown on ISP3 solid medium were washed with sterile water and adjusted to 10^8 CFU mL^{-1} using the hemacytometer method. All *Streptomyces* strains were tested for antagonistic activities against Rs1115 using the spot spray method on NA plates [61].

We constructed a synthetic community (SynCom) to simulate the rhizosphere microbiome of tomato plants. This SynCom consisted of 100 bacterial strains isolated from the tomato rhizosphere, representing different major genera to model the diversity and composition of the rhizosphere soil microbiome (for detailed community composition and abundances, see Table S5). These microbes were isolated using the same procedures as stated above. Briefly, the bacterial colonies were cultured on NA plates for purification and maintained in glycerol (15%, v/v) at −80℃ for long-term preservation. For SynCom construction, each strain was revived on NA plates, and single colonies were inoculated in nutrient broth and shaken at 30℃, 170 rpm for 24 h. Hereafter, each isolate (adjusted to OD_{600} = 0.5 using cells harvested from the exponential growing stage ~ 24–36 h) was mixed in equal volume, and the cells were harvested by centrifugation at 6000 rpm for 10 min, washed twice by sterile saline, and diluted to 10^8 CFU mL^{-1} based on the OD_{600} = 0.7.

Plant material and experimental soils

Tomato (*Lycopersicon esculentum* cv. "Red-Dwarf") was used as the model plant in this study. The seeds were provided by Beijing Dongsheng Seed Industry Co. LTD. Prior to the experiments, the seeds were surfaced and disinfected following these steps: first, they were soaked in sterile water for 16 h, then disinfected with 75% alcohol for 30 s. Afterwards, the seeds were rinsed with sterile water (4 times) and immersed in 10% NaOCl for 20 min. Finally, the seeds were thoroughly rinsed with sterile water (> 4 times), dried with sterile paper, and transferred to 1/2 Murashig and Skoog (MS) medium [64] for germination over 3 days. After germination, the seeds were planted in seedling trays, each containing 50 g of sterile seedling substrate (Jiangsu Xingnong Substrate Technology Co., LTD. Product No. 161102G0097 N) and grown in a greenhouse at 22–32℃, with 70% relative humidity and 16/8 h photoperiod under a Photosynthetic Photon Flux Density of 200 μmol m^{-2} s^{-1}. The plants were watered regularly with sterile water. Seventeen days after sowing (three-leaf stage), the plants were transplanted into sterile pots each containing either 100 g of sterile cultivation substrate (Jiangsu Xingnong Substrate Technology Co., LTD. Product No. 161102G0096 N) or 200 g

of field soil. The same greenhouse conditions were maintained and watered regularly with sterile water. The field soil (nature soil) used in this study was collected from an agricultural field in Qilin town, Nanjing, China (118° 57′ E, 32° 03′ N), which was free of *R. solanacearum* based on our previous findings [34]. The substrate was fully sterilized by gamma radiation before use.

Phylogenetic backgrounds and biological characterization of *Streptomyces* strains

The genomic DNA of *Streptomyces* spp. was extracted using Invitrogen PureLink® Genomic DNA kit. The PCR amplification of the 16S rRNA gene was performed using the universal primers 27 F (5′-AGAGTTTGATCATGG CTCAG-3′) and 1492R (5′-TACGGTTACCTTGTT ACGACTT-3′) [65]. The PCR products were sequenced by Shanghai BIOZERON Biotechnology Co., Ltd, and the obtained sequences were then analyzed using the EzBioCloud platform [66]. We also used the pyani software for average nucleotide identity (ANI) analysis to classify the whole genome of *Streptomyces* spp. [67, 68]. Detailed methods for whole bacterial genome sequencing and genome analyses of these *Streptomyces* spp. are provided in the supplementary materials.

The morphological characteristics of *Streptomyces* spp. were analyzed by light microscopy (Eclipse E200, Nikon) and scanning electron microscopy (SU8010 SEM, Hitachi, Japan). *Streptomyces* was cultured on ISP3 solid medium for 5 days. Fresh colonies were excised using a sterile blade into pieces ≤6 mm ×6 mm, thickness ≤2 mm, then fixed in 2.5% glutaraldehyde for over 8 h. The samples were washed three times with phosphate-buffered saline (10 min each) and dehydrated using an ethanol gradient (15 min each in 50%, 70%, 80%, and 90% ethanol; followed by three rounds of 30 min each in 100% ethanol). The samples were then replaced with tert-butanol 3 times (30 min each), freeze-dried, mounted on a sample stage with the observation surface facing upward, and sputter-coated with a 10-nm gold film. Spore morphology was then observed under SU8010 SEM (Hitachi, Japan). The samples for SEM were prepared as described by Jin et al. [69]. Color determination was done with color chips from the ISCC-NBS color charts [70]. Bacterial growth at different temperatures (5, 10, 15, 20, 25, 28, 32, 37, 40, 42, and 45 °C) was determined on ISP3 medium after incubation for 14 days. Growth tests for the pH range (4.0–12.0, at intervals of 1.0 pH unit) and tolerance of various NaCl concentrations (0–9%, with an interval of 1%, w/v) were tested in glucose yeast extract medium (GY medium) (1% glucose, 1% yeast extract, 0.05% $K_2HPO_4{\cdot}3H_2O$, 0.05% $MgSO_4{\cdot}7H_2O$, w/v; pH 7.2) at 28℃ for 2 weeks [71]. Hydrolyses of Tweens (20, 40, and 80) and production of urease were tested as described by Smibert et al. (1994) [72]. The utilization of sole carbon and nitrogen sources, hydrolysis of starch, reduction of nitrate, decomposition of cellulose, liquefaction of gelatin, and production of H_2S, IAA, and urease were examined following standard procedures [73–75]. To assess *Streptomyces* colonization in the tomato rhizosphere, we used a sterile cultivation system. Tomato seedlings were grown on the sterile substrate, and 10 mL of spore suspension (10^8 CFU/mL) was applied to the roots. Each treatment had three replicates, with rhizosphere samples collected on days 10, 20, and 30. For plate counting, 5 g of air-dried, ground soil was suspended in 45-mL sterile water with glass beads, shaken at 280 rpm for 12–20 min at 28 °C, and serially diluted. Two hundred microliters of aliquots from 10^{-3}, 10^{-4}, and 10^{-5} dilutions were plated on KHI medium with 0.1% actinomycin and 0.1% naphthalene acid, then incubated in the dark at 28 °C for 5–7 days. To confirm strain identity, colonies were initially selected based on morphology and color, followed by liquid culturing and 16S rRNA sequencing, ensuring no contaminants were present. The colonization of *Streptomyces* in the rhizosphere was evaluated by quantifying the number of individual colonies using a serial dilution and plate counting method.

Effects of *Streptomyces* spp. on the wilt disease in nature soil

We conducted a greenhouse experiment to test the protective ability of *Streptomyces* spp. on the bacterial wilt of tomatoes in a natural soil environment. The experiment comprised 52 treatments, including *Streptomyces* (50 treatments inoculated with both Rs1115 and different individual strains of *Streptomyces* spp.), Rs (inoculated only with Rs1115), and healthy control (not inoculated with any microbes). Tomato seedlings (*Lycopersicon esculentum* cv. "Red-Dwarf") were prepared as described previously. After 17 days of growth on seeding trays containing sterile substrates, tomato plants with similar sizes were transferred to six-cell plant trays filled with ~200 g natural soil per cell. Seven days after transplantation, 50 individual strains of *Streptomyces* were inoculated to the roots of each plant at a density of 1.0×10^7 CFU g^{-1} soil. Seven days after inoculation with *Streptomyces*, Rs1115 was inoculated to the roots at a final density of 1.0×10^6 CFU g^{-1} soil. Each treatment consisted of three biological replicates (seedling trays) and each biological replicate contained six tomato plants (a total of 18 plants per treatment resulting in a total of 936 plants for the experiment). Tomato plants were cultivated and managed under the same conditions as previously described. At 50 days post-Rs1115 inoculation, the disease level was recorded, which ranged from 0 to 4 (0, no wilting; 1, 1–25% of leaf area wilted; 2, 26–50% of leaf area wilted;

3, 51–75% of leaf area wilted; and 4, 76–100% of leaf area wilted). The disease rate (DR) was calculated following the formula:

$$DR = \frac{\text{The number of diseased plants}}{\text{Total number of surveyed plants}} \times 100\%$$

The Disease Index (DI) was calculated following the formula:

$$\text{DI} = \frac{\sum(Nd \times Cd)}{Ts \times Ad} \times 100$$

where *Nd* is the number of diseased plants at the given disease level, *Cd* is the corresponding disease level, *Ts* is the total number of plants surveyed, and *Ad* is the actual highest disease level. The biocontrol efficiency (BE) was calculated following the formula:

$$\text{BE} = \frac{\text{DI}_{\text{CK}} - \text{DI}_{\text{T}}}{\text{DI}_{\text{CK}}} \times 100\%$$

where DI_{CK} is the disease index of Rs1115 treatment, and DI_T is the disease index of *Streptomyces* treatments [76, 77].

In this study, the DR measures the proportion of infected plants, indicating disease prevalence without considering severity. The DI combines both disease rate and severity for a comprehensive impact assessment. BE measures the extent of disease suppression, serving as an indicator of biocontrol effectiveness.

Effects of *Streptomyces* spp. on the wilt disease in a SynCom context

To investigate how *Streptomyces* controls wilt disease and affects rhizosphere microbiomes, with or without the SynCom, we selected the twelve *Streptomyces* strains with superior biocontrol efficiency (ranging from 68% to 100%) to conduct a targeted greenhouse experiment. The seedling substrate and cultivation substrate were sterilized by gamma irradiation to eliminate natural microbes and minimize their impact. A total of 27 treatments were included: 12 individually selected *Streptomyces* strains against Rs (-SynCom), 12 individually selected *Streptomyces* strains combined with the SynCom against Rs (+SynCom), Rs (inoculated with Rs1115 only), and healthy (not inoculated with any microbes).

We used tomato seedlings (*Lycopersicon esculentum* cv. "Red-Dwarf") prepared as previously described. Briefly, 17-day-old seedlings grown on sterile substrates of similar sizes were transferred to six-cell plant trays containing 100 g of sterile substrate per cell. Seven days post-transplantation, we inoculated the *Streptomyces* to the roots at a density of 1.0×10^7 CFU g^{-1} soil. For the *Streptomyces*+ SynCom treatments, both the SynCom and *Streptomyces* were inoculated at the same density. After seven more days, Rs1115 was also introduced to the roots at a density of 1.0×10^6 CFU g^{-1} soil. Each treatment consisted of three biological replicates with six plants per replicate, resulting in a total of 486 plants being used for the experiment. The plant growth conditions and methods for disease evaluation are referred to in previous descriptions.

Development of the SynCom database for enhanced microbial sequencing and analysis

The SynCom database was then constructed to facilitate accurate microbial diversity sequencing and comparison by providing a tailored sequence library of 12 selected *Streptomyces* strains and SynCom members, reducing interference from external microbes and ensuring precise mapping and abundance determination of the included species. The SynCom database was constructed using 16S rRNA sequences derived from the complete genomes of 122 individual strains, encompassing 100 distinct species. All 122 complete genomes were sequenced using a combination of PacBio RS and Illumina sequencing platforms. We used ABySS [78] to perform genome assembly with multiple-Kmer parameters to achieve optimal results of the assembly. Subsequently, canu [79] was used to assemble the PacBio corrected long reads and GapCloser ("https://sourceforge.net/projects/soapdenovo2/files/GapCloser/") was subsequently applied to fill up the remaining local inner gaps and correct the single base polymorphism for the final assembly results. To extract 16S rRNA sequences of each genome, 16S rRNA was determined using the RNAmmer (v1.2) [80]. Then, one full-length 16S rRNA sequence was extracted from each identified region to construct the SynCom database. Additionally, cd-hit (v 4.5.7, −c 1.0 −n 5− M 0) was employed to ensure the uniqueness of the sequences within the SynCom database. Taxonomic IDs and corresponding taxonomic classifications for each species were established by conducting BLAST searches of the 16S rRNA sequences against the NCBI database.

Rhizosphere sample collection, DNA extraction, and amplicon sequencing

We analyzed the assembly of the tomato rhizosphere microbiome in response to resistance against Rs1115 induced by *Streptomyces* spp. Rhizosphere samples from the treatment combining *Streptomyces* and SynCom were collected 15 days post Rs1115 inoculations. The entire tomato was carefully uprooted from the pot, and the loose soil was shaken off. The soil adhering to the roots was then scraped off using a sterile scraper and transferred to a sterile ziplock bag for storage at −80℃. Rhizosphere samples from the 12 *Streptomyces*+ SynCom treatments and one SynCom treatment were collected.

The gDNA was extracted from these rhizosphere samples using the E.Z.N.A.® Soil DNA Kit (Omega Bio-tek, Norcross, GA, U.S.) according to the manufacturer's protocols. The V4-V5 region of the bacteria 16S ribosomal RNA gene was amplified by PCR using primers F515 (5′-GTGCCAGCMGCCGCGG- 3′) and R907 (5′-CCGTCAATTCMTTTRAGTTT- 3′) [81]. PCR reactions were performed in triplicate using a 20-μL system consisting of 4 μL of 5× FastPfu buffer, 2 μL of 2.5 mM dNTPs, 0.8 μL of each primer (5 μM), 0.4 μL of FastPfu Polymerase, and 10 ng of template DNA. Thermal conditions were 95 °C for 2 min, followed by 25 cycles at 95 °C for 30 s, 55 °C for 30 s, and 72 °C for 30 s and a final extension at 72 °C for 5 min [81]. Amplicons were cut from 2% agarose gels and purified using the AxyPrep DNA Gel Extraction Kit (Axygen Biosciences, Union City, CA, USA) according to the manufacturer's instructions. Negative controls for DNA extraction and PCR amplification were included to prevent false-positive results. Sequencing was performed using the Illumina MiSeq platform (CA, USA). The raw reads were deposited into the NCBI Sequence Read Archive (SRA) database under the accession number PRJNA1123384.

The raw sequencing files were demultiplexed using in-house perl scripts according to the barcode sequences information for each sample with the following criteria: (i) The 250bp reads were truncated at any site receiving an average quality score < 20 over a 10 bp sliding window, discarding the truncated reads that were shorter than 50 bp. (ii) Exact barcode matching was required, allowing for a maximum of 2 nucleotide mismatches in primer matching, reads containing ambiguous characters were excluded. (iii) Only sequences with overlaps longer than 10 bp were assembled according to their overlap sequence. Reads that could not be assembled were discarded. Subsequently, the passed sequences were dereplicated and subjected to the DADA2 algorithm to identify indel-mutations and substitutions [82]. Trimming and filtering were performed on paired reads with a maximum of two expected errors per read (maxEE = 1). Following the merging of paired reads and chimera filtering, phylogenetic affiliation of each 16S rRNA gene sequence was analyzed by BLAST ("https://blast.ncbi.nlm.nih.gov/Blast.cgi") against the SynCom database using the threshold of *e*-value < 1×10^{-10} and identity > 90% [83, 84].

Quantification of the pathogen density in soil samples using qPCR method

The *fliC* gene encodes a flagellar subunit and is a reliable marker for PCR-based detection of the pathogen Rs1115 due to its conserved structure and location at the end of a variable central region [85]. The structure of the flagellin gene is conserved, located at the end of a variable central region. The qPCR assays were performed using the Applied Biosystems 7500 real-time PCR system (Applied Biosystems, CA, USA) with primers specific to *fliC* (forward: 5′-GAACGCCAACGGTGCGAACT- 3′; reverse: 5′-GGCGGCCTTCAGGGAGGTC- 3′) [85]. Each 20 μL reaction mixture contained 10 μL SYBR premix Ex Taq (TaKaRa Bio Inc.), 2 μL of DNA template, and 0.4 μL of each primer (10 mM each). The thermal cycling conditions were as follows: an initial denaturation at 95 °C for 30 s, followed by 40 cycles of 95 °C for 5 s and 60 °C for 34 s. Melt curve analysis was performed, with steps including 95 °C for 15 s, 60 °C for 1 min, and 95 °C for 15 s. Each sample was analyzed in triplicate. Standard curves were constructed using a cloned *fliC* gene from Rs1115 inserted into the pMD19-T vector (Takara, Dalian, China), following procedures described in our previous study [86]. The pathogen density in the rhizosphere was expressed as *R. solanacearum fliC* gene copy numbers per gram of dry soil [87], with calculations based on the method described by Whelan et al. [88].

Determining interactions between *Streptomyces* R02, keystone species of SynCom, and the pathogen Rs1115 using supernatant cross-feeding assay

To quantify the type and direction of each pairwise interaction among *Streptomyces* spp. and keystone species and Rs1115. We examined the effects of *Streptomyces* R02, treated with bacterial supernatants on Rs1115 growth, which was collected from a low-resource (20% NB) medium [89]. To obtain the supernatants, microbial cultures were grown in 20% NB medium for 24 h at 30 °C, 170 rpm, in darkness (shaker covered with black plastic). The cultures were then diluted to OD_{600} = 0.5 using a SpectraMax M5 plate reader (Molecular Devices, Sunnyvale, CA, USA), centrifuged (7000 rpm, 10 min, 4℃) and filter-sterilized (Millex-GP Filter, 0.22 μm, PES membrane, SLGPR33RB) to remove living cells. All OD measurements and storage were conducted in darkness to minimize light-induced compound degradation. Subsequently, 10 mL of sterile supernatant from each strain's culture and 1 mL spore suspension of *Streptomyces* R02 (density of 10^7 cells mL^{-1}) was inoculated into 90 mL of fresh 100% NB medium at 170 rpm, 30℃. After 7 days of *Streptomyces* R02 growth, the sterile supernatant was obtained by the same method. Following this, 20 μL of sterile supernatant from each treatment and 2 μL overnight culture of Rs1115 (OD_{600} = 0.5) were inoculated into separate tubes containing 180 μL of fresh 20% NB medium (to better reflect the effect of the supernatant). Control treatments were inoculated with 20 μL of 20% NB media instead of the supernatant, inoculated with 20 μL sterile supernatant from *Streptomyces* R02 (same growth conditions but not affected by bacterial

supernatants) of 20% NB media, and inoculated with 20 µL sterile water of 20% NB media. The control treatments were inoculated with Rs1115 in the same way, and each treatment was conducted in 12 replicates. We used a similar method as described above to determine the effects of *Streptomyces* R02's supernatant on CSC98 and CSC13, the interactions between bacterial CSC98 and CSC13, the effect of these two bacterial supernatants on *Streptomyces* R02 and their collective effects on Rs1115.

Pairwise interactions between keystone taxa and Rs1115

Due to distinct differences in colony morphology among the bacterial strains (CSC98 and CSC13) and Rs1115, we then tested the growth of three bacterial stains alone or in the presence of the other species using a two-species co-culture system [90]. Monocultures were inoculated at an initial density of 10^5 cells mL^{-1} (bacterial densities were determined by plating on NA plates, followed by counting to confirm the density and adjusting to 10^5 cells mL^{-1}), while co-cultures were inoculated at half of this density for each species, and the inoculation was standardized to 1.0% of the final culture volume, following established protocols [89]. These experiments were carried out in NB using 12-well plates (2 mL per well), incubated at 30℃ with shaking at 170 rpm for 24 h. After incubation, the bacterial growth was quantified as colony-forming units (CFU) per mL by serial dilution and plating on NA plates.

Transcriptomic analysis of *Streptomyces* R02 and CSC13_R02 cells

Twelve microbial cell samples (R02, and CSC13_R02, six replicates each) were prepared for transcriptome sequencing. The total RNA was extracted from cell tissues using TRIzol® Reagent (Invitrogen) following the manufacturer's instructions, and genomic DNA was removed using DNase (TaKara). Paired-end libraries were sequenced on the Illumina NovaSeq 6000 platform (150bp*2, Shanghai BIOZERON Co., Ltd). The raw paired-end reads were trimmed and quality controlled by Trimmomatic (v0.36) with parameters of SLIDINGWINDOW: 4:15 and MINLEN:75. Clean reads were aligned to the reference genome with orientation mode using Rockhopper software [91–93]. Differential gene expression analysis was performed using the DESeq2 R package (v1.22.1) [94]. The resulting gene *P*-values were adjusted using Benjamini and Hochberg's method to control the false discovery rate (FDR). Genes with a $\log_2$ fold change (Log_2FC) > 1, and FDR < 0.05 were considered differentially expressed. Kyoto Encyclopedia of Genes and Genomes (KEGG) pathway analyses were performed using the KEGG Orthology-Based Annotation System (KOBAS version 3.0) (http://kobas.cbi.pku.edu.cn/kobas3) to reveal the functions of the differentially expressed genes.

Metabolomic analysis of microbial supernatant samples using LC–MS/MS

Eighteen microbial metabolic supernatant samples (CSC13+R02, CSC13 only, and R02 only, six replicates each) were prepared for metabolomic extraction and transcriptome analysis. Briefly, the supernatant samples were initially collected via centrifugation at 12,000 rpm at 4℃ for 10 min. The supernatants, stored at −80℃, were then thawed and vortexed for 30 s to mix. A 9-mL aliquot of the sample was transferred to a fresh 50-mL centrifuge tube, frozen at −80 ℃ overnight, and vacuum freeze-dried. After freeze-drying, a 70% methanolic internal standard extract was added at a ratio of 30 times the freeze-dried product, vortexed for 15 min, and sonicated in an ice water bath (KQ5200E) for 10 min. It was then centrifuged at 4℃ and 12,000 rpm for 3 min, and the resulting supernatant was filtered through a 0.22-µm microporous membrane and stored in the injection vial for LC–MS/MS detection. Details on LC–MS/MS conditions and metabolomic analysis are provided in the supplementary materials of this study.

Determination of the antibacterial activity of Erythromycin E against Rs1115

A single colony of Rs1115 was selected from the NA plate and cultured overnight in an NB medium. The following day, the bacterial suspension was centrifuged (6000 rpm for 10 min) to remove the supernatant, and the resulting pellet was resuspended in sterile water. The OD_{600} of the suspension was adjusted to 0.5. Erythromycin E, supplied by Hebei Baiwei Precision Plant Extract Co., Ltd., was diluted in DMSO to concentrations of 256 µg/mL, 128 µg/mL, 32 µg/mL, 16 µg/mL, 8 µg/mL, 4 µg/mL, 2 µg/mL, 0.5 µg/mL, 0.25 µg/mL, and 0.125 µg/mL. The Oxford cup method was then employed on NA plates to assess antibacterial activity. An aliquot of 100 µL of the above concentration of Erythromycin E was loaded into each Oxford cup. An equal volume of DMSO and NB medium were included as controls. All these treatments were then tested for antagonistic activities against Rs1115, using the spot spray method to inoculate Rs1115 on NA plates.

Additionally, Erythromycin E solution of different concentrations was added to the NB medium at a proportion of 10%. Rs1115 suspension with $OD_{600} = 0.5$ was inoculated at 1% and cultured for 24 h to test OD_{600}. The minimum inhibitory concentration (MIC) was defined as the minimum concentration of the inhibitory zone or OD_{600} below that of the DMSO controls. Each treatment was performed with four technical replicates.

Statistical analysis

All analyses were conducted in R version 4.2.2. Alpha diversity of microbial communities was calculated by package vegan [95]. The impacts of *Streptomyces* spp. on rhizosphere microbiomes and their effects on disease severity and pathogen density were evaluated using two-way ANOVA. Principal coordinates analysis (PCoA) based on Bray-Curtis distances was performed to assess the effect of *Streptomyces* spp. on the rhizosphere microbiome composition using the vegan package [96]. The differences in bacterial community composition between treatments were tested using permutational multivariate analysis of variance (PERMANOVA; Adonis, transformed data by Bray-Curtis, permutations = 999). The heatmap was drawn using http://www.omicshare.com. The schematic illustration summarizing the experimental design of this study was drawn using https://www.biorender.com. Co-occurrence network analysis was conducted between *Streptomyces* spp. and SynCom to specifically focus on the members of the SynCom that responded to *Streptomyces* spp. and were involved in disease inhibition following the Molecular Ecological Network Analyses Pipeline (MENA) [97], then visualized by Gephi software (version 0.9.2) [98]. This random matrix theory (RMT)-based approach enables differentiation of genuine, system-specific microbial associations from random noise without relying on arbitrary thresholds, which is well-suited to sequencing datasets [98]. Prior to network analysis, we retained only those ASVs present in at least 50% of replicates across all samples to enhance consistency and reliability. To address compositional constraints inherent in microbiome data, we applied a centered log-ratio (CLR) transformation, which normalizes the data, stabilizes variance, and significantly reduces the risk of spurious correlations. Spearman correlation was subsequently used for the construction of microbial correlation networks. Finally, we manually validated selected key microbial interactions, such as those involving CSC13, CSC98, Rs1115, and *Streptomyces*, to confirm the reliability of the inferred associations. The microbes influenced by *Streptomyces* spp. and significantly enriched were then determined by the DESeq2 generalized linear model, using alpha = 0.05 to exclude false positives. We determined significantly enriched species by applying a corrected P-value < 0.05 and a $\log_2$ fold change > 1 [94]. When comparing mean differences between treatments, we used analysis of variance (Tukey's multiple ranges) and Student's t-test or Welch's t-test (for samples with unequal variances or unequal sample size), where $P \leq 0.05$ was considered statistically significant.

Supplementary Information

The online version contains supplementary material available at https://doi.org/10.1186/s40168-025-02120-y.

Additional file 1: Figure S1. Schematic illustration summarizing the experimental design of this study. (a) Greenhouse experiments evaluated the ability of 50 *Streptomyces* strains to inhibit bacterial wilt disease in natural soils; twelve of these strains with the high biocontrol efficiency. (b) and (c) Layout of greenhouse experiments involving twelve selected *Streptomyces* isolates, conducted with and without the synthetic community (SynCom). These experiments involved treating plants with the 12 *Streptomyces* strains across 18 replicates to assess disease resistance in relation to bacterial treatment and subsequent microbial community profiling. (d) Examination of interactions between *Streptomyces* R02 and key SynCom members through coculturing tests using respective bacterial culture supernatants. (e) The mechanism of Rs inhibition by key SynCom members and *Streptomyces* R02 was elucidated through transcriptomic and metabolomic analyses. Figure S2 The phylogenetic tree, constructed using the maximum-likelihood algorithm based on 16S rRNA gene sequences, showing the genetic relationships between 50 strains of *Streptomyces* species (including *Streptomyces asenjonii* R02) used in this study. Figure S3 The greenhouse experiment evaluating twelve strains of *Streptomyces* (R02, R08, R11, R17, R21, R28, R33, R35, R39, R41, R44, and Y1) for their efficacy against bacterial wilt disease on tomato plants in natural soil. Plants marked with red flags indicate disease presence. R02-R44, and Y1: *Streptomyces* strains inoculated against *Ralstonia solanacearum* on the plant. Rs: only the pathogen *Ralstonia solanacearum* was inoculated. Healthy: no microbial inoculation; DR: disease rate; DI: disease index; BE: biocontrol efficiency. Detailed method for calculation of the DR, DI and BE, please refer to the Material and Methods. Number of replicates per treatment = 18. Figure S4 Phylogenetic analysis and morphological characteristics of the 12 *Streptomyces* strains. (a) The phylogenetic tree constructed using the maximum-likelihood algorithm based on 16S rRNA gene sequences, showing the genetic relationships of the 12 *Streptomyces* strains. Branch lengths are proportional to genetic distances, indicating evolutionary divergence. (b) Colony morphology and scanning electron microscopy (SEM) images of the *Streptomyces* strains, showing their distinct morphological traits. The left panels show morphology of single colonies grown on ISP3 solid medium for 7 days, while the right panels present high-resolution SEM images of the spore chains and mycelial structures of each strain. Figure S5 Greenhouse experiment testing the effectiveness of twelve *Streptomyces* strains against bacterial wilt disease in tomato plants using a sterile cultivation substrate. Plants marked with a red circle are diseased. 'RXX/Y1' denotes inoculation with different *Streptomyces* strains for combating *Ralstonia solanacearum*. 'Rs' indicates inoculation with the *Ralstonia solanacearum* strain alone. 'Healthy' represents plants not inoculated with any microbes. 'DR' stands for disease rate, and 'DI' represents disease index. For detailed methods on calculation of DR and DI, please refer to the Material and Methods. Number of replicates per treatment = 18. Figure S6 Greenhouse experiment testing the effectiveness of twelve *Streptomyces* strains combined with a synthetic community (SynCom) for resistance against bacterial wilt disease in a sterile cultivation substrate. Plants marked with red circles indicate those that are diseased. The treatment labels are as follows: RXX/Y1+SynCom denotes inoculation with different *Streptomyces* strains combined with SynCom to combat *Ralstonia solanacearum*; Rs indicates inoculation with only the *Ralstonia solanacearum* strain; Healthy represents plants that were not inoculated with any microbes; SynCom denotes plants inoculated only with the synthetic community. DR: disease rate, DI: Disease Index. Figure S7 Scatter plot showing the relationship between inhibition zone size (cm) on agar plates and biocontrol efficiency (%) on tomato plants grown in sterile cultivation substrate without the synthetic community (SynCom) for the 12 *Streptomyces* strains. The x-axis represents the antagonistic effect of each strain against *Ralstonia solanacearum*, while the y-axis indicates the corresponding biocontrol efficiency (%) in the absence of SynCom. Data points are color-coded to represent different *Streptomyces* strains. The R^2 and P-value showed a non-significant correlation between inhibition zone size and biocontrol efficiency. Figure S8 (related to Figure 2 d). An DESeq

analysis showing differential ASV abundances between the treatments of SynCom alone and SynCom combined with different *Streptomyces* strains. Each subplot represents a specific *Streptomyces* strain (R02, R08, R11, R17, R21, R28, R33, R35, R39, R41, R44, Y1) combined with the SynCom. The right section (red points) shows members of the SynCom significantly enriched in relative abundances under the *Streptomyces* treatments, while the left section (blue points) shows those ASVs significantly reduced in relative abundance. The gray points represent ASVs with non-significant changes. Figure S9 (related to Figure 4e). Interactions between CSC13, CSC98 with the pathogen Rs1115 on nutrient agar plates. (A) The central spot was inoculated with CSC13 and (B) CSC98, respectively, with the surrounding bacterial colonies are the pathogen. Figure S10 Differential gene expression analysis and KEGG pathway enrichment between R02 and CSC13_R02 groups. (a) Heatmap of differentially expressed genes (DEGs) clustered based on Z-score values. Each column represents individual samples from two groups, R02 and CSC13_R02, and the hierarchical clustering shows distinct gene expression patterns between the two groups. (b) The DESeq analysis showing the distribution of DEGs between CSC13_R02 and R02 groups. The red and green dots represent significantly upregulated (762 genes) and downregulated (1153 genes) DEGs, respectively, with dotted lines indicating significance thresholds. (c) Top 25 KEGG pathway enrichment analysis for the DEGs, ranked based on enrichment significance, with different levels of statistical significance marked by * ($P < 0.05$), ** ($P < 0.01$), and *** ($P < 0.001$). Figure S11 Metabolomic profiling and enrichment analysis comparing CSC13+R02 and R02 only groups. (a) Pie chart showing the classification of detected metabolites across different biochemical categories including the major metabolic groups of amino acids and derivatives (33.74%), organic acids (11.28%), and nucleotides and derivatives (10.34%). (b) Heatmap of metabolite abundance based on Z-score values across samples from CSC13+R02, R02 only, and CSC13 only groups, and the hierarchical clustering of metabolites reveals distinct patterns of metabolite accumulation across the different groups. (c) Bubble plot of enriched KEGG metabolic pathways, with the bubble size corresponding to the number of metabolites involved in each pathway, and color indicates statistical significance (*P*-value). (d) OPLS-DA (orthogonal partial least squares-discriminant analysis) score plot showing differences between the metabolomic profiles of the CSC13+R02 and R02 only groups, with clear separation observed. (e) Permutation test results for OPLS-DA model validation. The bar graph shows the distribution of R^2Y and Q^2Y values, confirming the robustness of the model with significant *p*-values (< 0.005) and high predictive accuracy ($Q^2 = 0.98$, $R^2Y = 0.999$). Figure S12 Joint analyses of metabolites and gene expressions by comparing CSC13_R02 with R02 only. (a) Workflow of the co-culture experiment of CSC13 and R02. Microbial metabolites in supernatants were filtered and analysed, with comparisons made between CSC13+R02 and R02 only groups. (b) Changes in metabolic and genetic pathways of *Streptomyces* R02 after treatment with the supernatant of CSC13, involved in six key KEGG pathways, (i) Biosynthesis of 12-,14- and 16-membered macrolides and related pathways, (ii) inositol phosphate metabolism, (iii) phenylalanine metabolism, (iv) pinene, camphor and geraniol degradation, (v) valine, leucine and isoleucine degradation, and (vi) glycolysis/gluconeogenesis (refer to the legend on the left for details). Genes upregulated in CSC13_R02 are marked in red, and dashed arrows represent biosynthesis links to key metabolites of Erythromycin E. (c) Bar chart showing enriched key genes in CSC13_R02 relative to R02 only. Significant differences are marked by asterisks (**$P < 0.01$, ***$P < 0.001$), with genes such as *katG*,*DLAT* and *acdH* showing significant upregulations in the co-culture condition. Figure S13 Other bacteriostatic-related secondary metabolites produced by *Streptomyces* R02. The table provides an overview of the three secondary metabolites, detailing their names, classifications, and structural characteristics. (a) Box plots show the content of secondary metabolite Rosmarinic acid among the three treatments ($F_{(2,15)} = 14.21$, $P < 0.001$, ANOVA). (b) Box plots show the content of secondary metabolite Quercetin among the three treatments ($F_{(2,15)} = 60.98$, $P < 0.001$, ANOVA). (c) Box plots show the content of secondary metabolite Paromomycin among the three treatments ($F_{(2,15)} = 10.66$, $P = 0.001$, ANOVA).

Additional file 2: Supplementary Dataset 1. The information of the fifty *Streptomyces* strains. The table showed fifty *Streptomyces* strains ID in this study and species taxonomy, the average diameters of inhibition zone against of *Ralstonia solanacearum* and their 16S rRNA sequences. The data of Average inhibition zone (cm) comes from the reference of yang et al [34]. Supplementary Dataset 2: The physiological characteristics of the twelve *Streptomyces* strains and their resistance to Rs when combined with SynCom or applied alone under sterile substrate conditions. The table showed twelve *Streptomyces* strains spore chain morphology and surface propa, aerial mycelium and substrate hyphae color, growth temperature range, pH range, salt tolerance, enzyme activity, rhizosphere colonization ability, carbon and nitrogen source utilization (+ positive, - negative) and the disease rate, disease index, biocontrol efficiency of *Streptomyces*+SynCom and *Streptomyces* only. Supplementary Dataset 3:The data of the whole genome sequencing of twelve *Streptomyces* strains. Supplementary Dataset 4:The Average Nucleotide Identity (ANI) analysis revealed the genomic proximity among twelve strains of *Streptomyces*. Supplementary Dataset 5: The data of the members of Synthetic community. The table showed CSC ID and strains ID of the members of Synthetic Community in this study and species taxonomy and their 16S rRNA. Supplementary Dataset 6: Results of 16S rRNA amplicon sequencing for rhizosphere microbial diversity in a greenhouse experiments combining *Streptomyces* and SynCom. Microbial relative abundance data for each treatment. Supplementary Dataset 7: The alpha diversity indices and PCoA1 and PCoA2 values of 12 *Streptomyces* combined with SynCom and SynCom alone in the glass house experiment. Note: SynCom: SynCom alone, R02: R02 combined with SynCom, R08: R08 combined with SynCom, R11: R11 combined with SynCom, R17: R17 combined with SynCom, R21: R21 combined with SynCom, R28: R28 combined with SynCom, R33: R33 combined with SynCom, R35: R35 combined with SynCom, R39: R39 combined with SynCom, R41: R41 combined with SynCom, R44: R44 combined with SynCom. Y1: Y1 combined with SynCom. Supplementary Dataset 8 (related to Fig 3a): Macro correlation network node data of twelve strains of *Streptomyces* and all members of the SynCom. Note: *Streptomyces*: strain R11, R35, R28, R08, R39, R17, R02, Y1, R44, R33, R41, R21 are collectively referred to as *Streptomyces*. Supplementary Dataset 9 (related to Fig 3a): Macro correlation network edge data of twelve strains of *Streptomyces* and all members of the SynCom. Note: *Streptomyces*: strain R11, R35, R28, R08, R39, R17, R02, Y1, R44, R33, R41, R21 are collectively referred to as *Streptomyces*. Supplementary Dataset 10 (related to Fig 4): The data of the metabolite-based interactions experiments between *Streptomyces* R02, key species CSC13 and CSC98, and Rs1115. The table showed the data of the effects of *Streptomyces* R02 on the growth of strains CSC13 and CSC98, the effects of strains CSC13 and CSC98 on mutual growth, co-culture of strain CSC13 and CSC98 with Rs1115, effects of supernatants from strains CSC98 and CSC13 on the growth of *Streptomyces* R02, impact of supernatants from various strains and their combinations (excluding *Streptomyces* R02) on Rs1115 growth, effects of single and combined bacterial supernatants on Rs1115's inhibition by *Streptomyces* R02 supernatant. Supplementary Dataset 11 (related to Fig S10a,b): Analysis of differential gene expression in *Streptomyces* R02 under the influence of metabolites produced by *P. cellulositrophicus* CSC13 (R02: *Streptomyces* R02 only; CSC13_R02: *Streptomyces* R02 under the influence of metabolites produced by *P. cellulositrophicus* CSC13, ND: no data of K_ID). Supplementary Dataset 12 (related to Fig 5b, Fig S10c): The KEGG enrichment analysis conducted for all significantly upregulated genes. Supplementary Dataset 13 (related to Fig S11a): All identified compounds of the metabolomic analysis. Note: CSC13+R02: Metabolite produced by *Streptomyces* R02 under *P. cellulositrophicus* CSC13 treatment; CSC13 only: Metabolites produced by the strain CSC13; R02 only: Metabolites produced by strain R02. (In the table, Erythromycin E is marked in red and other antimicrobial related secondary metabolites are marked in yellow). Supplementary Dataset 14: The significant differences in metabolites between the treatment CSC13+R02 and the control R02 only. Note: CSC13+R02: Metabolites produced by *Streptomyces* R02 under *P. cellulositrophicus* CSC13 treatment; R02 only: Metabolites produced by strain R02. Supplementary Dataset 15 (related to Fig 6): Erythromycin E exhibits bactericidal activity against Rs1115 (The data of inhibition zone and OD_{600}).

Acknowledgements
Not applicable.

Authors' contributions
Z.W., Y.C.X., X.F.W. and S.M.W. conceived the project and designed the experiments. T.Y.S. and M.C.H. conducted the experiments. T.Y.S., H.W.L. and N.Q.W. performed the statistical analyses. T.Y.S., H.W.L., X.F.W. and Z.W. wrote the first draft, all authors discussed and commented on the results and on the manuscript.

Funding
This research was supported by the National Key Research and Development Program of China (2023YFD1701501, 2024YFC3406003), Fundamental Research Funds for the Central Universities (KJYQ2025034, KJYQ2024039, and KYT2023001), National Natural Scientific Foundation of China (42090064, 42325704, and 42377118), Natural Science Foundation of Jiangsu Province (BK20240194), Jiangsu Carbon Peak and Carbon Neutrality Science and Technology Innovation Special Fund (BE2022423), and China Postdoctoral Science Foundation (2024M760612).

Data availability
No datasets were generated or analysed during the current study.

Declarations

Ethics approval and consent to participate
Not applicable.

Consent for publication
Not applicable.

Competing interests
The authors declare no competing interests.

Author details
[1]Jiangsu Provincial Key Lab for Solid Organic Waste Utilization, Key Lab of Organic-Based Fertilizers of China, Jiangsu Collaborative Innovation Center for Solid Organic Wastes, Educational Ministry Engineering Center of Resource-saving fertilizers, Nanjing Agricultural University, Nanjing 210095, China. [2]College of Agro-Grassland Science, Nanjing Agricultural University, Nanjing, Jiangsu 210095, People's Republic of China. [3]Hawkesbury Institute for the Environment, Western Sydney University, Penrith, NSW 2753, Australia. [4]Department of Microbiological Sciences, North Dakota State University, Fargo, ND, USA.

Received: 16 November 2024 Accepted: 21 April 2025
Published online: 19 May 2025

References

1. Mendes R, Kruijt M, De Bruijn I, Dekkers E, Van Der Voort M, Schneider JH, et al. Deciphering the rhizosphere microbiome for disease-suppressive bacteria. Science. 2011;332(6033):1097–100. https://doi.org/10.1126/science.1203980.
2. Liu H, Brettell LE. Plant defense by VOC-induced microbial priming. Trends Plant Sci. 2019;24(3):187–9. https://doi.org/10.1016/j.tplants.2019.01.008.
3. Vejan P, Abdullah R, Khadiran T, Ismail S, Nasrulhaq BA. Role of plant growth promoting rhizobacteria in agricultural sustainability-a review. Molecules. 2016;21(5): 573. https://doi.org/10.3390/molecules21050573.
4. Chen XH, Koumoutsi A, Scholz R, Schneider K, Vater J, Süssmuth R, et al. Genome analysis of Bacillus amyloliquefaciens FZB42 reveals its potential for biocontrol of plant pathogens. J Biotechnol. 2009;140(1–2)(-):27–37. https://doi.org/10.1016/j.jbiotec.2008.10.011.
5. Du Y, Wang T, Jiang J, Wang Y, Lv C, Sun K, et al. Biological control and plant growth promotion properties of *Streptomyces albidoflavus* St-220 isolated from *Salvia miltiorrhiza* rhizosphere. Front Plant Sci. 2022;13: 976813. https://doi.org/10.3389/fpls.2022.976813.
6. Helepciuc FE, Todor A. EU microbial pest control: a revolution in waiting. Pest Manag Sci. 2022;78(4):1314–25. https://doi.org/10.1002/ps.6721.
7. Lahlali R, Ezrari S, Radouane N, Kenfaoui J, Esmaeel Q, El Hamss H, et al. Biological control of plant pathogens: a global perspective. Microorganisms. 2022;10(3): 596. https://doi.org/10.3390/microorganisms10030596.
8. Mark GL, Morrissey JP, Higgins P, O'gara F. Molecular-based strategies to exploit Pseudomonas biocontrol strains for environmental biotechnology applications. FEMS Microbiol Ecol. 2006;56(2):167-177. https://doi.org/10.1111/j.1574-6941.2006.00056.x.
9. Whipps JM. Microbial interactions and biocontrol in the rhizosphere. J Exp Bot. 2001;52:487–511. https://doi.org/10.1093/jexbot/52.suppl_1.487.
10. Berg G, Kusstatscher P, Abdelfattah A, Cernava T, Smalla K. Microbiome modulation-toward a better understanding of plant microbiome response to microbial inoculants. Front Microbiol. 2021;12: 650610. https://doi.org/10.3389/fmicb.2021.650610.
11. Gu S, Wei Z, Shao Z, Friman VP, Cao K, Yang T, et al. Competition for iron drives phytopathogen control by natural rhizosphere microbiomes. Nat Microbiol. 2020;5(8):1002–10. https://doi.org/10.1038/s41564-020-0719-8.
12. Morris JJ, Johnson ZI, Szul MJ, Keller M, Zinser ER. Dependence of the *Cyanobacterium Prochlorococcus* on hydrogen peroxide scavenging microbes for growth at the ocean's surface. PLoS ONE. 2011;6(2): e16805. https://doi.org/10.1371/journal.pone.0016805.
13. Schiering N, Kabsch W, Moore MJ, Distefano MD, Walsh CT, Pai EF. Structure of the detoxification catalyst mercuric ion reductase from Bacillus sp. strain RC607. Nature. 1991;352(6331):168–72. https://doi.org/10.1038/352168a0.
14. She W, Ye W, Shi Y, Zhou L, Zhang Z, Chen F, et al. A novel chresdihydrochalcone from Streptomyces chrestomyceticus exhibiting activity against Gram-positive bacteria. Journal of Antibiotics. 2020;73(7):429. https://doi.org/10.1038/s41429-020-0298-1.
15. Gu JQ, Alexander DC, Rock J, Brian P, Chu M, Baltz RH. Structural characterization of a lipopeptide antibiotic A54145E(Asn3Asp9) produced by a genetically engineered strain of *Streptomyces fradiae*. J Antibiot. 2011;64(1):111–6. https://doi.org/10.1038/ja.2010.140.
16. Mee MT, Collins JJ, Church GM, Wang HH. Syntrophic exchange in synthetic microbial communities. Proc Natl Acad Sci. 2014;111(20):E2149–56. https://doi.org/10.1073/pnas.1405641111.
17. Li Y, Guo Q, Li Y, Sun Y, Xue Q, Lai H. *Streptomyces pactum* act12 controls tomato yellow leaf curl virus disease and alters rhizosphere microbial communities. Biol Fertil Soils. 2019;55(2):149–69. https://doi.org/10.1007/s00374-019-01339-w.
18. Niehus R, Oliveira NM, Li A, Fletcher AG, Foster KR. The evolution of strategy in bacterial warfare via the regulation of bacteriocins and antibiotics. Elife. 2021;10: e69756. https://doi.org/10.7554/eLife.69756.
19. Shepherdson EMF, Baglio CR, Elliot MA. *Streptomyces* behavior and competition in the natural environment. Curr Opin Microbiol. 2023;71: 102257. https://doi.org/10.1016/j.mib.2022.102257.
20. Xun W, Liu Y, Li W, Ren Y, Xiong W, Xu Z, et al. Specialized metabolic functions of keystone taxa sustain soil microbiome stability. Microbiome. 2021;9(1): 35. https://doi.org/10.1186/s40168-020-00985-9.
21. Wang M, Liu X, Nie Y, Wu XL. Selfishness driving reductive evolution shapes interdependent patterns in spatially structured microbial communities. ISME J. 2021;15(5):1387–401. https://doi.org/10.1038/s41396-020-00858-x.
22. Getzke F, Hassani MA, Crüsemann M, Malisic M, Zhang P, Ishigaki Y, et al. Cofunctioning of bacterial exometabolites drives root microbiota establishment. Proc Natl Acad Sci. 2023;120(15): e2221508120. https://doi.org/10.1073/pnas.2221508120.
23. Singh K, Chandra R, Purchase D. Unraveling the secrets of rhizobacteria signaling in rhizosphere. Rhizosphere. 2022;21: 100484. https://doi.org/10.1016/j.rhisph.2022.100484.
24. Ahmad R, Tousif MI, Nazir M, Yaqoob A, Shah SA, Zengin G, et al. Marine Streptomyces sp. PGC 39: a treasure trove of new antimicrobial agents, macrolidycin, and pyrachlomycin. Food. Bioscience. 2024;57:103600. https://doi.org/10.1016/j.fbio.2024.103600.
25. Castillo U, Harper JK, Strobel GA, Sears J, Alesi K, Ford E, et al. Kakadumycins, novel antibiotics from *Streptomyces* sp NRRL 30566, an endophyte of *Grevillea pteridifolia*. FEMS Microbiol Lett. 2003;224(2):183–90. https://doi.org/10.1016/S0378-1097(03)00426-9.
26. Ezra D, Castillo UF, Strobel GA, Hess WM, Porter H, Jensen JB, et al. Coronamycins, peptide antibiotics produced by a verticillate Streptomyces sp. (MSU-2110) endophytic on Monstera sp. Microbiology. 2004;150(4):785–93. https://doi.org/10.1099/mic.0.26645-0.

27. Narayana KJ, Peddikotla P, Krishna PS, Yenamandra V, Muvva V. Indole-3-acetic acid production by *Streptomyces albidoflavus*. J Biol Res-Thessaloniki. 2009;11:49–55. http://hdl.handle.net/123456789/7097.
28. Olanrewaju OS, Babalola OO. *Streptomyces*: implications and interactions in plant growth promotion. Appl Microbiol Biotechnol. 2019;103:1179–88. https://doi.org/10.1007/s00253-018-09577-y.
29. El-Tarabily KA. Promotion of tomato (Lycopersicon esculentum Mill.) plant growth by rhizosphere competent 1-aminocyclopropane-1-carboxylic acid deaminase-producing streptomycete actinomycetes. Plant and Soil. 2008;308:161–74. https://doi.org/10.1007/s11104-008-9616-2.
30. Sui J, Ji C, Wang X, Liu Z, Sa R, Hu Y, et al. A plant growth-promoting bacterium alters the microbial community of continuous cropping poplar trees' rhizosphere. J Appl Microbiol. 2019;126(4):1209–20. https://doi.org/10.1111/jam.14194.
31. Krespach MK, Stroe MC, Netzker T, Rosin M, Zehner LM, Komor AJ, et al. *Streptomyces* polyketides mediate bacteria-fungi interactions across soil environments. Nat Microbiol. 2023;8(7):1348–61. https://doi.org/10.1038/s41564-023-01382-2.
32. Savary S, Willocquet L, Pethybridge SJ, Esker P, McRoberts N, Nelson A. The global burden of pathogens and pests on major food crops. Nature ecology and evolution. 2019;3(3):430–9. https://doi.org/10.1038/s41559-018-0793-y.
33. Chevrette MG, Carlson CM, Ortega HE, Thomas C, Ananiev GE, Barns KJ, et al. The antimicrobial potential of *Streptomyces* from insect microbiomes. Nat Commun. 2019;10(1):516. https://doi.org/10.1038/s41467-019-08438-0.
34. Yang K, Fu R, Feng H, Jiang G, Finkel O, Sun T, et al. RIN enhances plant disease resistance via root exudate-mediated assembly of disease-suppressive rhizosphere microbiota. Mol Plant. 2023. https://doi.org/10.1016/j.molp.2023.08.004.
35. Li G, Liu T, Xie W, Liu Z, Li H, Whalen JK, et al. Metabolites limiting predator growth wane with prey biodiversity. Proc Natl Acad Sci. 2024;121(52): e2410210121. https://doi.org/10.1073/pnas.2410210121.
36. Banerjee S, Schlaeppi K, van der Heijden MG. Keystone taxa as drivers of microbiome structure and functioning. Nat Rev Microbiol. 2018;16(9):567–76. https://doi.org/10.1038/s41579-018-0024-1.
37. Kim JD, Han JW, Lee SC, Lee D, Hwang IC, Kim BS. Disease control effect of strevertenes produced by *Streptomyces psammoticus* against tomato Fusarium wilt. J Agric Food Chem. 2011;59(5):1893–9. https://doi.org/10.1021/jf1038585.
38. Fajardo A, Martínez JL. Antibiotics as signals that trigger specific bacterial responses. Curr Opin Microbiol. 2008;11(2):161–7. https://doi.org/10.1016/j.mib.2008.02.006.
39. Kost C, Patil KR, Friedman J, Garcia SL, Ralser M. Metabolic exchanges are ubiquitous in natural microbial communities. Nat Microbiol. 2023;8(12):2244–52. https://doi.org/10.1038/s41564-023-01511-x.
40. Bonaldi M, Chen X, Kunova A, Pizzatti C, Saracchi M, Cortesi P. Colonization of lettuce rhizosphere and roots by tagged *Streptomyces*. Front Microbiol. 2015;6: 25. https://doi.org/10.3389/fmicb.2015.00025.
41. Martin JR, Devault RL, Sinclair AC, Stanaszek RS, Johnson P. A new naturally occurring erythromycin: erythromycin F. J Antibiotics. 1982;35(4):426–30. https://doi.org/10.7164/antibiotics.35.426.
42. Dey P, Hossain I, Mahmud H, Hossain, MD. Management of seed borne *Ralstonia solanacearum* in brinjal (*Solanum melongena* L.) and tomato (*Lycopersicon esculentum* Mill.). Bangladesh J Bot. 2024;53(1):173–83. https://doi.org/10.3329/bjb.v53i1.72279.
43. Orlewska K, Piotrowska-Seget Z, Bratosiewicz-Wąsik J, Cycoń M. Characterization of bacterial diversity in soil contaminated with the macrolide antibiotic erythromycin and/or inoculated with a multidrug-resistant Raoultella sp. strain using the PCR-DGGE approach. Applied Soil Ecology. 2018;126:57–64. https://doi.org/10.1016/j.apsoil.2018.02.019.
44. Shen D, Gu X, Zheng Y, Delgado-Moreno L, Jia W, Ye Q, et al. The fate of erythromycin in soils and its effect on soil microbial community structure. Sci Total Environ. 2022;820: 153373. https://doi.org/10.1016/j.scitotenv.2022.153373.
45. Zhao R, Feng J, Liu J, Fu W, Li X, Li B. Deciphering of microbial community and antibiotic resistance genes in activated sludge reactors under high selective pressure of different antibiotics. Water Res. 2019;151:388–402. https://doi.org/10.1016/j.watres.2018.12.034.
46. Berg G, Marten P, Ballin G. *Stenotrophomonas maltophilia* in the rhizosphere of oilseed rape-occurrence, characterization and interaction with phytopathogenic fungi. Microbiol Res. 1996;151(1):19–27. https://doi.org/10.1016/S0944-5013(96)80051-6.
47. Ryan RP, Monchy S, Cardinale M, Taghavi S, Crossman L, Avison MB, et al. The versatility and adaptation of bacteria from the genus *Stenotrophomonas*. Nat Rev Microbiol. 2009;7(7):514–25. https://doi.org/10.1038/nrmicro2163.
48. Berendsen RL, Vismans G, Yu K, Song Y, de Jonge R, Burgman WP, et al. Disease-induced assemblage of a plant-beneficial bacterial consortium. ISME J. 2018;12(6):1496–507. https://doi.org/10.1038/s41396-018-0093-1.
49. Liu H, Li J, Carvalhais LC, Percy CD, Prakash Verma J, Schenk PM, et al. Evidence for the plant recruitment of beneficial microbes to suppress soil-borne pathogens. New Phytol. 2021;229:2873–85. https://doi.org/10.1111/nph.17057.
50. Cao ZJ, Zhang Q, Wei DK, Chen L, Wang J, Zhang XQ, et al. Characterization of a novel *Stenotrophomonas* isolate with high keratinase activity and purification of the enzyme. J Ind Microbiol Biotechnol. 2009;36(2):181–8. https://doi.org/10.1007/s10295-008-0469-8.
51. Minkwitz A, Berg G. Comparison of antifungal activities and 16S ribosomal DNA sequences of clinical and environmental isolates of *Stenotrophomonas maltophilia*. J Clin Microbiol. 2001;39(1):139–45. https://doi.org/10.1128/jcm.39.1.139-145.2001.
52. Grady EN, MacDonald J, Liu L, Richman A, Yuan ZC. Current knowledge and perspectives of *Paenibacillus*: a review. Microb Cell Fact. 2016;15:1–8. https://doi.org/10.1186/s12934-016-0603-7.
53. Ahmad M, Hussain A, Dar A, Luqman M, Ditta A, Iqbal Z, et al. Combating iron and zinc malnutrition through mineral biofortification in maize through plant growth promoting *Bacillus* and *Paenibacillus* species. Front Plant Sci. 2023;13: 1094551. https://doi.org/10.3389/fpls.2022.1094551.
54. Fürnkranz M, Adam E, Müller H, Grube M, Huss H, Winkler J, et al. Promotion of growth, health and stress tolerance of Styrian oil pumpkins by bacterial endophytes. Eur J Plant Pathol. 2012;134:509–19. https://doi.org/10.1007/s10658-012-0033-2.
55. de Souza R, Meyer J, Schoenfeld R, da Costa PB, Passaglia LM. Characterization of plant growth-promoting bacteria associated with rice cropped in iron-stressed soils. Annals of microbiology. 2015;65:951–64. https://doi.org/10.1007/s13213-014-0939-3.
56. Weselowski B, Nathoo N, Eastman AW, MacDonald J, Yuan ZC. Isolation, identification and characterization of *Paenibacillus polymyxa* CR1 with potentials for biopesticide, biofertilization, biomass degradation and biofuel production. BMC Microbiol. 2016;16:1–10. https://doi.org/10.1186/s12866-016-0860-y.
57. Hertlein G, Müller S, Garcia-Gonzalez E, Poppinga L, Süssmuth RD, Genersch E. Production of the catechol type siderophore bacillibactin by the honeybee pathogen *Paenibacillus larvae*. PLoS ONE. 2014;9(9): e108272. https://doi.org/10.1371/journal.pone.0108272.
58. Jin X, Jia H, Ran L, Wu F, Liu J, Schlaeppi K, et al. Fusaric acid mediates the assembly of disease-suppressive rhizosphere microbiota via induced shifts in plant root exudates. Nat Commun. 2024;15(1):5125. https://doi.org/10.1038/s41467-024-49218-9.
59. Ram RM, Keswani C, Bisen K, Tripathi R, Singh SP, Singh HB. Biocontrol technology: eco-friendly approaches for sustainable agriculture. Omics Technologies and Bio-Engineering. 2018;177–190. https://doi.org/10.1016/B978-0-12-815870-8.00010-3.
60. Niu B, Wang W, Yuan Z, Sederoff RR, Sederoff H, Chiang VL, et al. Microbial interactions within multiple-strain biological control agents impact soil-borne plant disease. Front Microbiol. 2020;11: 585404. https://doi.org/10.3389/fmicb.2020.585404.
61. Wei Z, Yang X, Yin S, Shen Q, Ran W, Xu Y. Efficacy of Bacillus-fortified organic fertiliser in controlling bacterial wilt of tomato in the field. Appl Soil Ecol. 2011;48(2):152–9. https://doi.org/10.1016/j.apsoil.2011.03.013.
62. Wang W, Ge Q, Wen J, Zhang H, Guo Y, Li Z, et al. Horizontal gene transfer and symbiotic microorganisms regulate the adaptive evolution of intertidal algae, Porphyra sense lato. Communications Biology. 2024;7(1):976. https://doi.org/10.1038/s42003-024-06663-y.
63. Shirling ET, Gottlieb D. Methods for characterization of *Streptomyces* species. Int J Syst Evol Microbiol. 1966;16(3):313–40. https://doi.org/10.1099/00207713-16-3-313.

64. Murashige T, Skoog F. A revised medium for rapid growth and bioassays with tobacco tissue cultures. Physiologia plantarum. 1962;15(3):473. https://doi.org/10.1111/j.1399-3054.1962.tb08052.x.
65. Heuer H, Krsek M, Baker P, Smalla K, Wellington E. Analysis of actinomycete communities by specific amplification of genes encoding 16S rRNA and gel-electrophoretic separation in denaturing gradients. Appl Environ Microbiol. 1997;63(8):3233–41. https://doi.org/10.1128/aem.63.8.3233-3241.1997.
66. Yoon SH, Ha SM, Kwon S, Lim J, Kim Y, Seo H, et al. Introducing EzBioCloud: a taxonomically united database of 16S rRNA gene sequences and whole-genome assemblies. Int J Syst Evol Microbiol. 2017;67(5):1613–7. https://doi.org/10.1099/ijsem.0.001755.
67. Richter M, Rosselló-Móra R. Shifting the genomic gold standard for the prokaryotic species definition. Proc Natl Acad Sci. 2009;106(45):19126–31. https://doi.org/10.1073/pnas.0906412106.
68. Pritchard L, Glover RH, Humphris S, Elphinstone JG, Toth IK. Genomics and taxonomy in diagnostics for food security: soft-rotting enterobacterial plant pathogens. Anal Methods. 2015;8(1):12–24. https://doi.org/10.1039/C5AY02550H.
69. Jin L, Zhao Y, Song W, Duan L, Jiang S, Wang X, et al. Streptomyces inhibens sp. nov. a novel actinomycete isolated from rhizosphere soil of wheat (Triticum aestivum L.). Int J Syst Evol Microbiol. 2019;69(3):688–95. https://doi.org/10.1099/ijsem.0.003204.
70. Kelly KL. Color-name charts illustrated with centroid colors. Inter-society color council-national bureau of standards, U.S. National Bureau of Standards: Washington, DC, USA. 1965.
71. Fu Y, Yan R, Liu D, Jiang S, Cui L, Guo X, et al. Trinickia diaoshuihuensis sp. nov. a plant growth promoting bacterium isolated from soil. Int J Syst Evol Microbiol. 2019;69(1):291–6. https://doi.org/10.1099/ijsem.0.003155.
72. Smibert RM, Krieg NR. Phenotypic characterization. In: Gerhardt P, Murray RGE, Wood WA, Krieg NR, editors. Methods for General and Molecular Bacteriology. Washington, DC: American Society for Microbiology; 1994. p. 607–54.
73. Gordon RE, Barnett DA, Handerhan JE, Pang CH. *Nocardia coeliaca*, *Nocardia autotrophica*, and the *Nocardin* Strain. Int J Syst Evol. 1974;24(1):54–63. https://doi.org/10.1099/00207713-24-1-54.
74. Yokota A, Tamura T, Hasegawa T, Huang LH. Catenuloplanes japonicus gen. nov., sp. nov., nom. rev., a new genus of the order Actinomycetales. Int J Syst Evol Microbiol. 1993;43(4):805–12. https://doi.org/10.1099/00207713-43-4-805.
75. Reineke G, Heinze B, Schirawski J, Buettner H, Kahmann R, Basse CW. Indole-3-acetic acid (IAA) biosynthesis in the smut fungus *Ustilago maydis* and its relevance for increased IAA levels in infected tissue and host tumour formation. Mol Plant Pathol. 2008;9(3):339–55. https://doi.org/10.1111/j.1364-3703.2008.00470.x.
76. Tans-Kersten J, Brown D, Allen C. Swimming motility, a virulence trait of *Ralstonia solanacearum*, is regulated by FlhDC and the plant host environment. Mol Plant Microbe Interact. 2004;17(6):686–95. https://doi.org/10.1094/MPMI.2004.17.6.686.
77. Guo JH, Qi HY, Guo YH, Ge HL, Gong LY, Zhang LX, et al. Biocontrol of tomato wilt by plant growth-promoting rhizobacteria. Biol Control. 2004;29(1):66–72. https://doi.org/10.1016/S1049-9644(03)00124-5.
78. Simpson JT, Wong K, Jackman SD, Schein JE, Jones SJ, Birol I. ABySS: a parallel assembler for short read sequence data. Genome Res. 2009;19(6):1117–23. https://doi.org/10.1101/gr.089532.108.
79. Koren S, Walenz BP, Berlin K, Miller JR, Bergman NH, Phillippy AM. Canu: scalable and accurate long-read assembly via adaptive k-mer weighting and repeat separation. Genome Res. 2017;27(5):722–36. https://doi.org/10.1101/gr.215087.116.
80. Lagesen K, Hallin P, Rødland EA, Stærfeldt HH, Rognes T, Ussery DW. RNAmmer: consistent and rapid annotation of ribosomal RNA genes. Nucleic Acids Res. 2007;35(9):3100–8. https://doi.org/10.1093/nar/gkm160.
81. Zhou J, Wu L, Deng Y, Zhi X, Jiang YH, Tu Q. Reproducibility and quantitation of amplicon sequencing-based detection. ISME J. 2011;5(8):1303–13. https://doi.org/10.1038/ismej.2011.11.
82. Callahan BJ, McMurdie PJ, Rosen MJ, Han AW, Johnson AJ, Holmes SP. DADA2: High-resolution sample inference from Illumina amplicon data. Nat Methods. 2016;13(7):581–3. https://doi.org/10.1038/nmeth.3869.
83. Mai Y, Zheng J, Zeng J, Wang Z, Liu F, Ma L, et al. Protozoa as hotspots for potential pathogens in the drinking water of a subtropical megacity: diversity, treatment, and health risk. Environ Sci Technol. 2023;57(15):6108–18. https://doi.org/10.1021/acs.est.2c09139.
84. Yang X, Jiang G, Zhang Y, Wang N, Zhang Y, Wang X, et al. MBPD: a multiple bacterial pathogen detection pipeline for One Health practices. Imeta. 2023;2(1): e82. https://doi.org/10.1002/imt2.82.
85. Schonfeld J, Heuer H, Van Elsas JD, Smalla K. Specific and sensitive detection of *Ralstonia solanacearum* in soil on the basis of PCR amplification of *fliC* fragments. Appl Environ Microbiol. 2003;69(12):7248–56. https://doi.org/10.1128/AEM.69.12.7248-7256.2003.
86. Cao Y, Zhang Z, Ling N, Yuan Y, Zheng X, Shen B, et al. *Bacillus subtilis* SQR 9 can control *Fusarium* wilt in cucumber by colonizing plant roots. Biol Fertil Soils. 2011;47(5):495–506. https://doi.org/10.1007/s00374-011-0556-2.
87. Hu J, Wei Z, Friman VP, Gu SH, Wang XF, Eisenhauer N, et al. Probiotic diversity enhances rhizosphere microbiome function and plant disease suppression. MBio. 2016;7:e01790–e01716. https://doi.org/10.1128/mbio.01790-16.
88. Whelan JA, Russell NB, Whelan MA. A method for the absolute quantification of cDNA using real-time PCR. J Immunol Methods. 2003;278(1–2):261–9. https://doi.org/10.1016/S0022-1759(03)00223-0.
89. Li M, Pommier T, Yin Y, Cao W, Zhang X, Hu J, et al. Resource availability drives bacteria community resistance to pathogen invasion via altering bacterial pairwise interactions. Environ Microbiol. 2022;24(12):5680–9. https://doi.org/10.1111/1462-2920.16184.
90. Foster KR, Bell T. Competition, not cooperation, dominates interactions among culturable microbial species. Curr Biol. 2012;22(19):1845–50. https://doi.org/10.1016/j.cub.2012.08.005.
91. Tjaden B. A computational system for identifying operons based on RNA-seq data. Methods. 2020;176:62–70. https://doi.org/10.1016/j.ymeth.2019.03.026.
92. De TB. novo assembly of bacterial transcriptomes from RNA-seq data. Genome Biol. 2015;16:1–10. https://doi.org/10.1186/s13059-014-0572-2.
93. McClure R, Balasubramanian D, Sun Y, Bobrovskyy M, Sumby P, Genco CA, et al. Computational analysis of bacterial RNA-seq data. Nucleic Acids Res. 2013;41(14): e140. https://doi.org/10.1093/nar/gkt444.
94. Love MI, Huber W, Anders S. Moderated estimation of fold change and dispersion for RNA-seq data with DESeq2. Genome Biol. 2014;15:1–21. https://doi.org/10.1186/s13059-014-0550-8.
95. Dixon P. VEGAN, a package of R functions for community ecology. J Veg Sci. 2003;14(6):927–30. https://doi.org/10.1111/j.1654-1103.2003.tb02228.x.
96. Chen Y, Bonkowski M, Shen Y, Griffiths BS, Jiang Y, Wang X, et al. Root ethylene mediates rhizosphere microbial community reconstruction when chemically detecting cyanide produced by neighbouring plants. Microbiome. 2020;8(1):1–17. https://doi.org/10.1186/s40168-019-0775-6.
97. Deng Y, Jiang YH, Yang Y, He Z, Luo F, Zhou J. Molecular ecological network analyses. BMC Bioinformatics. 2012;13:1–20. https://doi.org/10.1186/1471-2105-13-113.
98. Bastian M, Heymann S, Jacomy M. Gephi: an open source software for exploring and manipulating networks. Proc Int AAAI Confer Web Soc Med. 2009;3(1):361–2. https://doi.org/10.1609/icwsm.v3i1.13937.

Publisher's Note